PHYSICAL REVIEW D **88,** 035025 (2013)

Natural supersymmetry and implications for Higgs physics

Graham D. Kribs,[1,2] Adam Martin,[3,4,*] and Arjun Menon[2]

[1]*School of Natural Sciences, Institute for Advanced Study, Princeton, New Jersey 08540, USA*
[2]*Department of Physics, University of Oregon, Eugene, Oregon 97403, USA*
[3]*PH-TH Department, CERN, CH-1211 Geneva 23, Switzerland*
[4]*Department of Physics, University of Notre Dame, Notre Dame, Indiana 46556, USA*

(Received 15 May 2013; published 29 August 2013)

We reanalyze the LHC bounds on light third-generation squarks in natural supersymmetry, where the sparticles have masses inversely proportional to their leading-log contributions to the electroweak symmetry breaking scale. Higgsinos are the lightest supersymmetric particles; top and bottom squarks are the next-to-lightest sparticles that decay into both neutral and charged Higgsinos with well-defined branching ratios determined by Yukawa couplings and kinematics. The Higgsinos are nearly degenerate in mass, once the bino and wino masses are taken to their natural (heavy) values. We consider three scenarios for the stop and sbottom masses: (I) $\tilde{t}_R$ is light; (II) $\tilde{t}_L$ and $\tilde{b}_L$ are light; and (III) $\tilde{t}_R$, $\tilde{t}_L$, and $\tilde{b}_L$ are light. Dedicated stop searches are currently sensitive to scenarios II and III but not scenario I. Sbottom-motivated searches ($2b$ + MET) impact both squark flavors due to $\tilde{t} \to b\tilde{\chi}_1^+$ as well as $\tilde{b} \to b\tilde{\chi}_{1,2}^0$, constraining scenarios I and III with somewhat weaker constraints on scenario II. The totality of these searches yields relatively strong constraints on natural supersymmetry. Two regions that remain are (1) the "compressed wedge," where $(m_{\tilde{q}} - |\mu|)/m_{\tilde{q}} \ll 1$ and (2) the "kinematic limit" region, where $m_{\tilde{q}} \gtrsim$ 600–750 GeV, at the kinematic limit of the LHC searches. We calculate the correlated predictions for Higgs physics, demonstrating that these regions lead to distinct predictions for the lightest Higgs couplings that are separable with $\simeq 10\%$ measurements. We show that these conclusions remain largely unchanged once the minimal supersymmetric standard model is extended to the nonminimal supersymmetric standard model in order to naturally obtain a large enough mass for the lightest Higgs boson consistent with LHC data.

DOI: 10.1103/PhysRevD.88.035025 PACS numbers: 14.80.Da, 12.60.Jv, 13.87.Ce

I. INTRODUCTION

Natural supersymmetry is the holy grail of beyond-the-standard-model physics. It contains a sparticle spectrum where sparticle masses are inversely proportional to their leading-log contributions to the electroweak symmetry breaking scale. At tree-level the electroweak symmetry breaking scale is determined by balancing the Higgsino mass-squared against the scalar Higgs mass-squareds. This implies the leading contribution to electroweak symmetry breaking comes from the Higgsino mass itself and thus implies the Higgsinos are the lightest sparticles in natural supersymmetry. The next largest contributions come from one-loop corrections from the stops. We consider the three scenarios: (I) $\tilde{t}_R$ is light; (II) $\tilde{t}_L$ and $\tilde{b}_L$ are light; and (III) $\tilde{t}_L$, $\tilde{t}_R$, and $\tilde{b}_L$ are light. This spans the space of possibilities for various stop (and sbottom) mass hierarchies consistent with natural supersymmetry. After this comes the contributions from the wino and gluino [in the minimal supersymmetric standard model (MSSM)], but their masses can be several times larger than the stop masses, given their comparatively suppressed contributions to electroweak symmetry breaking. Natural supersymmetry suggests the lightest electroweakinos can be nearly pure Higgsino-like states.

This spectrum is well-known [1–40], and the LHC experiments have already provided outstanding constraints on simplified models involving light stops [41–43], light sbottoms [44,45], and gluinos that decay into these sparticles [46–49]. Further improvement in the bounds may be possible with specialized search strategies; for recent examples, see Refs. [50–65]. However, the experimental results presented thus far typically make strong assumptions about branching fractions [$\mathrm{BR}(\tilde{t}_1 \to t\tilde{\chi}_1^0) = 1$ or $\mathrm{BR}(\tilde{t}_1 \to b\tilde{\chi}_1^\pm) = 1$].[1] In addition, in cases where both a light chargino and a light neutralino are present, the results assume certain mass hierarchies: $m_{\tilde{\chi}_1^\pm} = 0.75 m_{\tilde{t}_1} + 0.25 m_{\tilde{\chi}_1^0}$ [43] or $m_{\tilde{\chi}_1^\pm} = 2 \times m_{\tilde{\chi}_1^0}$ [41] or $m_{\tilde{\chi}_1^\pm} - m_{\tilde{\chi}_1^0} \gtrsim$ 50 GeV [41]. These assumptions make it difficult to extract the true bounds on natural supersymmetry. Consequently, we have undertaken a reevaluation of the

*Visiting scholar from Department of Physics, University of Notre Dame, Notre Dame, IN 46556, USA.

[1]The notable exceptions are the two recent ATLAS searches for $\tilde{t}_1 \to t\tilde{\chi}_1^0$ in the one-lepton mode [41] and all-hadronic mode [42], where constraints on the branching fraction $\mathrm{BR}(\tilde{t}_1 \to t\tilde{\chi}_1^0)$ were shown, assuming the remaining branching fraction is unobservable. Natural supersymmetry, however, predicts branching fractions into several channels that are observable, as we will see.

constraints on natural supersymmetry using the existing LHC results on simplified models involving light stops and sbottoms.

It is also well-known that there is an intricate interplay between a light third-generation and Higgs physics. Supersymmetry predicts the mass of the lightest Higgs boson to high accuracy through radiative corrections that are dominated by just the third-generation squarks [66–76]. If the third-generation squarks are collectively light (say, $\lesssim 1$ TeV), the predicted mass of the Higgs boson is too small to be compatible with the ATLAS and CMS observation [77,78] of a 125 GeV Higgs-like boson (e.g., Refs. [28,37,40,79–91]). On the other hand, light third-generation sparticles can significantly modify the detailed properties—production cross section and decay rates—of the lightest Higgs boson [92–105].

We consider the effects of natural supersymmetry on the detailed properties of the lightest Higgs boson. Here we are not interested in *maximizing* a particular decay channel or fitting to the existing Higgs results, but instead we endeavor to simply understand the characteristics that natural supersymmetry has on Higgs physics. Our main result is to overlay the modifications to the Higgs physics onto the allowed parameter space of natural supersymmetry. Two interesting regions emerge. In the "compressed wedge" region where $(m_{\tilde{q}} - |\mu|)/m_{\tilde{q}} \ll 1$ and $m_{\tilde{q}}$ can be small, the effects on Higgs physics are to enhance the inclusive (gluon-fusion–dominated) cross section $\sigma^{\text{incl}}_{\text{MSSM}}$ by 10–30% simultaneous with a slight reduction of $\text{BR}(h \to \gamma\gamma)_{\text{MSSM}}$ by up to 5%. By contrast, in the kinematic limit region where $m_{\tilde{q}} \gtrsim 600$–$750$ GeV, there is a slight enhancement of $\text{BR}(h \to \gamma\gamma)_{\text{MSSM}}$ by up to 5%, with the inclusive (gluon-fusion–dominated) cross section $\sigma^{\text{incl}}_{\text{MSSM}}$ within a few % of the Standard Model result. While the experimental situation among the LHC collaborations is not yet settled, it is already clear that these two regions lead to distinctly different effects on Higgs properties that can be probed with $\simeq 10\%$ measurements.

Given light stops and sbottoms, we must consider the supersymmetric prediction for the lightest Higgs boson mass. We assert that natural supersymmetry—in the MSSM—is simply *incompatible* with obtaining a lightest Higgs boson mass consistent with the LHC data. This point has been emphasized in some recent work, for example, Refs. [81,106,107]. Hence, we do not restrict the third-generation squark masses to obtain a given lightest Higgs boson mass. Instead, we assume there is another contribution to the quartic coupling that is sufficient to augment the MSSM contributions, resulting in a Higgs mass that matches the experiment, $m_h \simeq 125$ GeV. Not specifying this contribution would seem to be fatal flaw of our analysis. We show that simple extensions of the MSSM, in particular the next-to-minimal supersymmetric standard model (NMSSM), can give both a sufficient boost to the quartic coupling with negligible effects on the Higgsino mass spectrum and the decay chains that we consider here. Specific examples of NMSSM parameter choices that realize our assertion are given in Appendix A.

We do not consider the gluino in this paper. The gluino contributions to the electroweak symmetry breaking scale may be significant in the MSSM, given the existing searches that suggest the gluino must be heavier than 1–1.3 TeV, depending on the search strategy [46–49,108]. However, the size of the gluino contribution to electroweak symmetry breaking is model-dependent: A Dirac gluino has a substantially smaller contribution to the electroweak symmetry breaking scale compared with a Majorana gluino, when the leading-log enhancements are included, allowing a Dirac gluino to be substantially heavier [109–111]. In addition, the search strategies for a gluino depend on its Majorana or Dirac character. One of the most important search strategies—involving same-sign dileptons (such as Refs. [46,49]) does not provide a constraint on a Dirac gluino.

II. MASS HIERARCHY IN NATURAL SUPERSYMMETRY

A. Contributions to the electroweak scale

In the MSSM the electroweak symmetry breaking scale is determined by, at tree level [112],

$$\frac{1}{2}M_Z^2 = \frac{\tan^2\beta + 1}{\tan^2\beta - 1}\frac{m_{H_d}^2 - m_{H_u}^2}{2} - \frac{1}{2}m_{H_u}^2 - \frac{1}{2}m_{H_d}^2 - |\mu|^2. \tag{1}$$

In saying "contribution to the electroweak scale," it is understood that the supersymmetric and supersymmetry breaking parameters are adjusted to obtain the value already determined by experiment. Here we are interested in the *relative size* of $|\mu|$ and the loop corrections to the electroweak breaking scale, i.e., M_Z.

For $\tan\beta$ very near 1, the coefficient of the first term in Eq. (1) becomes large, because the D-flat direction in the scalar potential is not lifted, and thus implies increased sensitivity to the supersymmetric parameters. The sensitivity is most easily understood by eliminating dependence on $m_{H_d}^2$ using the tree-level relation [112]

$$m_A^2 = 2|\mu|^2 + m_{H_u}^2 + m_{H_d}^2 \tag{2}$$

to obtain

$$\frac{1}{2}M_Z^2 = \frac{1}{\tan^2\beta - 1}m_A^2 - \frac{\tan^2\beta + 1}{\tan^2\beta - 1}(m_{H_u}^2 + |\mu|^2). \tag{3}$$

At large $\tan\beta$, however, Eq. (3) simplifies to

$$\frac{1}{2}M_Z^2 = -m_{H_u}^2 - |\mu|^2 \tag{4}$$

and eliminates dependence on m_A^2. Generally, we have taken $\tan\beta = 10$ for the analyses to follow, and thus the heavy Higgs scalars that acquire masses near m_A can be

readily decoupled from our analysis. However, the smaller $\tan\beta$ region reappears in our discussion of the NMSSM in Appendix A, where the relative contributions to the electroweak symmetry breaking scale become more complicated for the NMSSM scalar potential.

With Eq. (4) in mind, we can compare the relative importance of different contributions to the electroweak symmetry breaking scale by normalizing to $M_Z^2/2$ [113]

$$\Delta(a^2) \equiv \left| \frac{a^2}{M_Z^2/2} \right|. \tag{5}$$

The tree-level and one-loop contributions are well-known (e.g., [37,112]),

$$\Delta(|\mu|^2) = 10 \times \frac{|\mu|^2}{(200\ \text{GeV})^2} \tag{6}$$

$$\begin{aligned}\Delta(\delta m_{H_u}^2|_{\text{stop}}) &= \frac{3y_t^2}{8\pi^2}(m_{Q_3}^2 + m_{u_3}^2 + |A_t|^2)\log\frac{\Lambda_{\text{mess}}}{(m_{\tilde{t}_1} m_{\tilde{t}_2})^{1/2}} \\ &\simeq 10 \times \frac{m_{Q_3}^2 + m_{u_3}^2 + |A_t|^2}{2 \times (450\ \text{GeV})^2} \\ &\quad \times \frac{\log \Lambda_{\text{mess}}/(m_{\tilde{t}_1} m_{\tilde{t}_2})^{1/2}}{3}.\end{aligned} \tag{7}$$

In the MSSM, there are also important one-loop contributions from a Majorana wino and two-loop contributions from a Majorana gluino (e.g., Refs. [37,112]),

$$\begin{aligned}\Delta(\delta m_{H_u}^2|_{\text{wino}}) &= \frac{3g_2^2}{8\pi^2}|M_2|^2 \log\frac{\Lambda_{\text{mess}}}{|M_2|} \\ &\simeq 10 \times \frac{|M_2|^2}{(930\,\text{GeV})^2}\frac{\log\Lambda_{\text{mess}}/|M_2|}{3}\end{aligned} \tag{8}$$

$$\begin{aligned}\Delta(\delta m_{H_u}^2|_{\text{gluino}}) &= \frac{2\alpha_s y_t^2}{\pi^3}|M_3|^2 \log\frac{\Lambda_{\text{mess}}}{(m_{\tilde{t}_1} m_{\tilde{t}_2})^{1/2}}\log\frac{\Lambda_{\text{mess}}}{|M_3|} \\ &= 10 \times \frac{|M_3|^2}{(1200\,\text{GeV})^2}\frac{\log\Lambda_{\text{mess}}/(m_{\tilde{t}_1} m_{\tilde{t}_2})^{1/2}}{3} \\ &\quad \times \frac{\log\Lambda_{\text{mess}}/|M_3|}{1.5}.\end{aligned} \tag{9}$$

Here we somewhat arbitrarily chose to normalize all of our numerical evaluations to a factor of 10 times $M_Z^2/2$, as well as normalizing the size of the leading logs to $\Lambda_{\text{mess}}/\tilde{m} = 20$.[2] This small ratio implicitly assumes a low scale for the messenger sector and thus the smallest sensitivity of supersymmetry breaking parameters to the electroweak breaking scale. This provides suggestive values for $|\mu|$, the stop masses, and in the MSSM, the wino and gluino masses. As these parameters significantly differ from these suggestive values, their relative importance to determining (or fine-tuning to determine) the electroweak scale is altered accordingly. In particular, we see that $|\mu| = 200$ GeV gives a comparable contribution to a pair of stops at $m_{\tilde{t}_1} = m_{\tilde{t}_2} = 450$ GeV.

The natural supersymmetry predictions for the wino and gluino mass depend on whether they acquire Majorana or Dirac masses. Already we see that if the wino acquires a Majorana mass, its mass is expected to be nearly 1 TeV. A Dirac wino would have a mass considerably larger. Similarly a Majorana gluino is expected to be 1.2 TeV (with the normalization of the logs as given above), and again significantly larger than this if it acquires a Dirac mass.

For the purposes of this paper, we assume the gluino is either sufficiently heavy so as to not lead to collider constraints (in practice, this means a Majorana gluino needs to be above about 1.3 TeV [46–49,108]), or it acquires a Dirac mass, in which case its natural supersymmetry mass is well out of range of the LHC. We assume the wino and bino acquires $\simeq 1$ TeV masses, but our results are largely insensitive to this choice.

B. Higgsino mass splitting

In the limit $M_{1,2} \gg |\mu|, v$, the lightest chargino and the lightest two neutralinos are Higgsino-like and nearly degenerate in mass. The leading contributions to the mass difference at order $1/M_{1,2}$ are

$$\begin{aligned}m_{\tilde{\chi}_1^\pm} - m_{\tilde{\chi}_1^0} &= \frac{M_W^2}{2M_2}\left(1 - \sin 2\beta - \frac{2\mu}{M_2}\right) \\ &\quad + \frac{M_W^2}{2M_1}\tan^2\theta_W(1 + \sin 2\beta)\end{aligned} \tag{10}$$

$$\begin{aligned}m_{\tilde{\chi}_2^0} - m_{\tilde{\chi}_1^0} &= \frac{M_W^2}{2M_2}\left(1 - \sin 2\beta + \frac{2\mu}{M_2}\right) \\ &\quad + \frac{M_W^2}{2M_1}\tan^2\theta_W(1 - \sin 2\beta),\end{aligned} \tag{11}$$

which we can write as

$$\begin{aligned}m_{\tilde{\chi}_1^\pm} - m_{\tilde{\chi}_1^0} &= (3.3\,\text{GeV})\left(\frac{1\,\text{TeV}}{M_2}\right)(1 - \sin 2\beta) \\ &\quad + (1.0\,\text{GeV})\left(\frac{1\,\text{TeV}}{M_1}\right)(1 + \sin 2\beta) \\ &\quad - (0.6\,\text{GeV})\left(\frac{\mu}{100\,\text{GeV}}\right)\left(\frac{1\,\text{TeV}}{M_2}\right)^2 \\ m_{\tilde{\chi}_2^0} - m_{\tilde{\chi}_1^0} &= (3.3\,\text{GeV})\left(\frac{1\,\text{TeV}}{M_2}\right)(1 - \sin 2\beta) \\ &\quad + (1.0\,\text{GeV})\left(\frac{1\,\text{TeV}}{M_1}\right)(1 - \sin 2\beta) \\ &\quad + (0.6\,\text{GeV})\left(\frac{\mu}{100\,\text{GeV}}\right)\left(\frac{1\,\text{TeV}}{M_2}\right)^2.\end{aligned}$$

[2]Except for $\Lambda_{\text{mess}}/|M_3| = \sqrt{20}$, since a conservative interpretation of LHC bounds is that the gluino already exceeds 1.3 TeV in viable scenarios.

Clearly, the mass differences among the Higgsinos are just a few GeV when $M_{1,2}$ take on natural (heavy) values. The decays $\tilde{\chi}_1^\pm, \tilde{\chi}_2^0 \to \tilde{\chi}_1^0$ thus yield unobservably small energy in the decay products. The mass difference is, however, large enough that the decay rates are prompt on collider time scales, and thus there are no macroscopic signatures in the detector (at least for wino and bino masses that do not far exceed $\simeq 1$ TeV). Hence, for the purposes of LHC detection, $\tilde{\chi}_1^\pm$, $\tilde{\chi}_{1,2}^0$ behave as neutral lightest supersymmetric particles that escape the detector as missing energy.

C. Simplified models of natural supersymmetry

Evidently from Eq. (7), the natural supersymmetry prediction for the stop masses depends on the sum $m_{Q_3}^2 + m_{u_3}^2 + |A_t|^2$. All other things considered equal, $A_t \neq 0$ implies the sum $m_{Q_3}^2 + m_{u_3}^2$ must be correspondingly smaller to hold the sum $m_{Q_3}^2 + m_{u_3}^2 + |A_t|^2$ constant. We therefore take A_t to vanish. While this might give some readers pause, regarding the stop contributions to the lightest Higgs mass, recall that we have already asserted that the MSSM is incapable of providing a sufficient contribution, and so the choice $A_t = 0$ is not inconsistent with our approach. Instead, we consider the following mass hierarchies ("scenarios") for natural supersymmetry: (I) $\tilde{t}_R$ is light; (II) $\tilde{t}_L$ and $\tilde{b}_L$ are light; and (III) $\tilde{t}_R$, $\tilde{t}_L$, and $\tilde{b}_L$ are light. These scenarios span the space of possibilities for the stop (and sbottom) masses. We illustrate these scenarios in Fig. 1. The resulting mass eigenstates are given by [112]

$$\text{Scenario I} \quad m_{\tilde{t}_1}^2 = m_{\tilde{u}_3}^2 + m_t^2 + \Delta_{\tilde{u}_R} \tag{12}$$

$$\text{Scenario II} \quad \begin{aligned} m_{\tilde{t}_1}^2 &= m_{\tilde{Q}_3}^2 + m_t^2 + \Delta_{\tilde{u}_L} \\ m_{\tilde{b}_1}^2 &= m_{\tilde{Q}_3}^2 + m_b^2 + \Delta_{\tilde{d}_L} \end{aligned} \tag{13}$$

$$\text{Scenario III} \quad \begin{aligned} m_{\tilde{t}_1}^2 &= m_{\tilde{Q}_3}^2 + m_t^2 + \Delta_{\tilde{u}_L} \\ m_{\tilde{t}_2}^2 &= m_{\tilde{u}_3}^2 + m_t^2 + \Delta_{\tilde{u}_R} \\ m_{\tilde{b}_1}^2 &= m_{\tilde{Q}_3}^2 + m_b^2 + \Delta_{\tilde{d}_L}, \end{aligned} \tag{14}$$

where $\Delta_{\tilde{q}} \equiv (T_q - Q_q \sin^2\theta_W)\cos(2\beta) M_Z^2$. In scenario III, we take the soft masses to be equal $m_{\tilde{Q}_3} = m_{\tilde{u}_3}$.[3] Since $\cos(2\beta) < 0$ for $\tan\beta > 1$, this implies $\Delta_{\tilde{u}_R} > 0$ whereas $\Delta_{\tilde{u}_L} < 0$, causing $\tilde{t}_1 \simeq \tilde{t}_L$ and $\tilde{t}_2 \simeq \tilde{t}_R$. Given that we specify soft masses, $\tilde{b}_1$ is always lighter than $\tilde{t}_1$ in scenarios II and III. The mass difference is (50, 30, 20) GeV for $m_{\tilde{Q}_3} = (200, 400, 600)$ GeV, corresponding to $(m_{\tilde{t}_1}, m_{\tilde{b}_1}) \simeq [(260, 210), (435, 405), (620, 600)]$ GeV. Finally, we also impose $m_{\tilde{Q}_3,\tilde{u}_3} - m_{\tilde{\chi}_1^0} > 50$ GeV for reasons related to the details of the search strategies employed by ATLAS and CMS. We discuss this in the next section.

[3]We also include the left-right squark mixing contribution $m_t\mu/\tan\beta$, but this is suppressed by our choice of $\tan\beta = 10$ as well as $m_t|\mu|$ being generally much smaller than $m_{\tilde{Q}_3}^2 = m_{\tilde{u}_3}^2$.

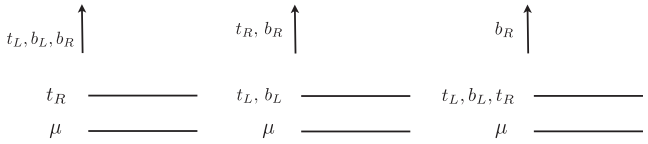

FIG. 1. The three scenarios of natural supersymmetry considered in this paper. Scenarios I, II, and III are illustrated in the left, middle, and right panels. In our study we varied $\mu \sim m_{\tilde{\chi}_1^0}$ between 100 and 500 GeV and lightest stop masses $m_{\tilde{t}_1} \sim 250$–1000 GeV.

All other gauginos, all sleptons, and the first- and second-generation squarks are taken to be sufficiently heavy that they do not play a role in the low-energy phenomenology, consistent with natural supersymmetry. We emphasize that the difference between scenarios I, II, and III is not that the stops are believed to be far different in mass but simply different enough in mass that the low-energy phenomenology is dominated by one of these three scenarios. Specifically, at the LHC the cross section for third-generation squark pair production drops by a factor of roughly 2 for every 50 GeV increase in mass. Thus, even a mass splitting among stops of only $\sim$200 GeV is sufficient to guarantee that LHC production is completely dominated by the lighter state.

III. COLLIDER BOUNDS ON NATURAL SUPERSYMMETRY

A. Collider study setup

The inputs for the spectra are the soft masses m_{Q_3}, m_{u_3}, m_{d_3}, the μ term, $\tan\beta$, the bottom and top Yukawas, and the weak scale v. For simplicity, we will assume the A_t, A_b terms are zero. However, by interpolating between our results for the three given scenarios, it is possible to reconstruct qualitatively what happens when $A_{t,b} \neq 0$. We set $\tan\beta = 10$, and any "decoupled" particle in a given scenario is, for purely practical reasons, taken to have mass 5 TeV. Our region of interest is $m_{\tilde{\chi}_1^0} > 100$ GeV, $m_{\tilde{t}_1} > 250$ GeV. The lower bound on the lightest supersymmetric particle (LSP) mass comes from the LEP bound on charginos—we must obey this bound since $m_{\tilde{\chi}_{1,2}^0} \sim m_{\tilde{\chi}_1^\pm} \sim \mu$. Finally, while the viability of stops with mass $\lesssim 250$ GeV remains an interesting question, we concentrate on $m_{\tilde{t}_1} > 250$ GeV, consistent with the natural supersymmetry spectrum.

We also impose an additional restriction on the parameter space, namely, to not let the mass difference between the squarks and the Higgsino become too small. The experimental analyses on stop production and decay through $\tilde{t} \to t\tilde{\chi}_1^0$ restricted $m_{\tilde{t}_1} - m_{\tilde{\chi}_1^0} > 175$ GeV for ATLAS semileptonic and all-hadronic searches [41,42] and >200 GeV for the CMS semileptonic search [43]. Stop decays in compressed spectra often lead to multiple-body final states that

are difficult to model without better tools. Additionally, the collider limits on nearly degenerate spectra become sensitive to how the additional radiation in the event (ISR) is modeled. We chose to simulate the sensitivity of these searches in natural supersymmetry for somewhat smaller mass differences, $m_{\tilde{Q}_3,\tilde{u}_3} - m_{\tilde{\chi}_1^0} > 50$ GeV. As we will see, we find the existing LHC searches are sensitive to natural supersymmetry with splittings this small. However, this region needs to be interpreted with some care, since we are obtaining constraints from both stop searches and sbottoms searches. Sbottom searches have somewhat different restrictions on the kinematics, but since we chose a minimum mass difference between the soft mass $m_{\tilde{Q}_3}$ and the lightest neutralino, the highly compressed region with respect to the sbottom and neutralino is not simulated. We therefore do not anticipate significant changes in the bounds for the parameter space we consider.

For each scenario at a given mass point $(\mu, m_{\tilde{q}})$, events are generated using PYTHIA6.4 [114]. We use CTEQ6L1 [115] parton distribution functions and take all underlying event and multiple interaction parameters to their values specified in Refs. [108,116]. The cross section is calculated by summing the next-to-leading order plus next-to-leading log (NLO + NLL) values [117–123] (using Ref. [124]) over all light ($<$ TeV) third-generation sparticles in the spectrum. Following PYTHIA generation, the events are fed into DELPHES [125] to incorporate detector geometry and resolution effects. We use the default DELPHES ATLAS and CMS detector descriptions but modify the jet definitions to agree with the corresponding experiment: anti-k_T algorithm, with size $R = 0.4$ for ATLAS and $R = 0.5$ for CMS analyses. Additionally, while the experimental flavor-tag/fake rates slightly differ from analysis to analysis, we used a fixed 70% tag rate for all b jets that lie in the tracker ($|\eta_j| < 2.5$).

The signal simulation is used to derive the efficiency—the survival rate in a given bin of a particular analysis. Given our simplified supersymmetry spectra, this efficiency is a function of the squark and LSP masses alone; i.e., for bin i, we find $\epsilon_i(m_{\tilde{t}_1}, m_{\tilde{\chi}_1^0})$. The product of the derived efficiency with the luminosity and the cross section (at NLO + NLL) is the number of signal events, s_i:

$$s_i = \mathcal{L} \times \sigma_{\mathrm{NLO+NLL}}(m_{\tilde{t}_1}) \times \epsilon_i(m_{\tilde{t}_1}, m_{\tilde{\chi}_1^0}).$$

We derive exclusion limits by comparing s_i at a given $(\tilde{m}_{\tilde{t}_1}, m_{\tilde{\chi}_1^0})$ with the number of signal events allowed at 95% C.L. calculated with a likelihood-ratio test statistic. Specifically, the 95% C. L. limit on the number of signal events, $s_{i,95}$, is the solution to

$$0.05 = \frac{\Pi_i \mathrm{Pois}(n_i|b_i + s_{i,95})}{\Pi_i \mathrm{Pois}(n_i|b_i)}, \tag{15}$$

where the n_i is the number of observed events in a channel i, b_i is the number of expected Standard Model background events, and we take the product over all orthogonal channels. We take both n_i and b_i directly from the experimental papers.

To incorporate systematic uncertainties, the number of background events in a bin is allowed to fluctuate: $b_i \to b_i(1 + \delta b_i)$. After multiplying by a Gaussian weighting factor, we integrate over δb_i, following Ref. [126]. We take the width of the Gaussian weighting factor to be the relative systematic uncertainty in a given bin quoted by the experiment, f_i^b, using the larger error if asymmetric errors are given,[4]

$$\mathrm{Pois}(n_i|b_i + s_{i,95}) \to \int \delta b_i \mathrm{Gaus}(\delta b_i, f_i^b)\mathrm{Pois}(n_i|b_i(1 + \delta b_i) + s_{i,95}). \tag{16}$$

One may ask if a likelihood-ratio analysis is really needed, instead of just a rescaling of existing bounds. If the signal yield according to ATLAS/CMS was given for each $(m_{\tilde{t}_1}, m_{\tilde{\chi}_1^0})$ bin, then we could rescale and determine the yield and thereby the exclusion bounds, in each of our scenarios. However, such detailed information is not public, and only the signal yields at specific benchmark points are given. In order to extrapolate yields away from the benchmarks, some model is needed, and for that we rely on the simulation method described above.

Before describing the details of the searches we consider, it is important to emphasize that the *absolute* bounds we present are only approximate. To derive the signal efficiency, we have used fast-simulation tools (DELPHES) whose energy smearing and tagging functions are approximations—usually optimistic—of the full detector effects. In multijet, especially multi–b-jet final states, the differences between the fast- and full-detector simulations add up, making it tricky for us to match the quoted absolute bounds on a given scenario. To improve the accuracy of the absolute bounds, the scenarios presented here should be studied by CMS/ATLAS themselves, either as a dedicated reanalysis or using a tool such as RECAST [127]. Meanwhile, the relative bounds, i.e. the difference between scenario I and scenario II, are robust.

B. Direct stop searches

In this section we present the limits on the supernatural scenarios from the most recent LHC direct stop searches [41–43]. Bounds from these searches are usually (though not always) cast in term of stops that decay either 100% of the time to a top quark and a neutralino or 100% of the time to a bottom quark and a chargino. Stops are searched for in several different final states, and the first two stop analyses we consider are semileptonic searches. While the details

[4]The Gaussian integration is truncated such that the number of background events is always positive.

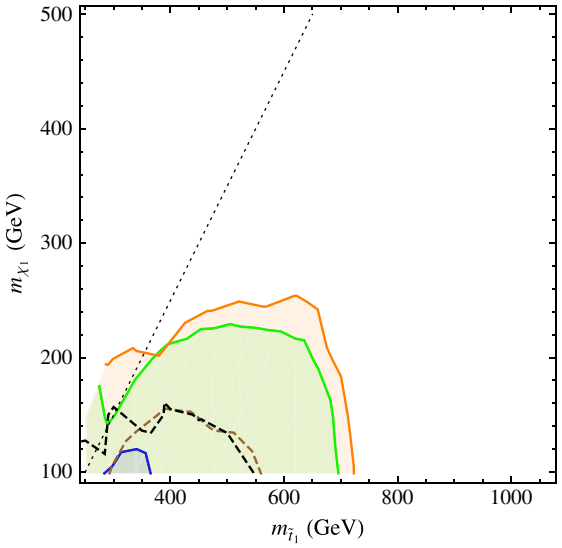

FIG. 2 (color online). Limits on the various third-generation scenarios coming from the CMS direct stop search (semileptonic channel). The x axis corresponds to the lightest physical stop mass $\tilde{t}_1$ in each scenario. In scenarios II and III, one b squark is present with a physical mass that is slightly lighter, given by Eq. (13). The orange contour shows the 95% exclusion bound on scenario III, the green contour is the bound on scenario II, and there is no bound on scenario I. The black, dashed contour is the bound from this analysis using CMS simplified model T2tt that involves direct production of stops which decay solely to unpolarized top plus neutralino; $\tilde{t}_1 \to t + \tilde{\chi}_1^0$. The brown dashed line shows the limit on a second default scenario: right-handed stops decaying to top plus bino. The difference between the black and brown dashed lines gives some indication how the polarization of the top can affect limits. The black dotted line is $m_{\tilde{t}} - m_{\tilde{\chi}_1^0} = 150$ GeV, which is the self-imposed restriction on the CMS analysis, since ISR is not properly taken into account when the signal is generated with PYTHIA. We have also restricted our reanalysis in the compressed wedge region [where $(m_{\tilde{q}} - m_{\tilde{\chi}_1^0})/m_{\tilde{q}} \ll 1$], requiring $m_{\tilde{Q}_3} - m_{\tilde{\chi}_1^0} > 50$ GeV, that results in the excluded region extending slightly to the left of the black dotted line. See the text for details.

differ between the ATLAS and CMS searches (see Appendix B for the full analyses description), both require a hard lepton, significant missing energy, and at least four jets, one of which must be tagged as a b jet.

Running our three scenarios through the CMS direct stop search [43], we find the following exclusion contours in the $(m_{\tilde{t}_1}, m_{\tilde{\chi}_1^0})$ plane (Fig. 2). This is somewhat an abuse of notation—the horizontal axis actually corresponds to the mass of the lightest stop eigenstate for a given spectra.[5] For comparison, we include limits from two "default" spectra (calculated in the same manner as our three scenarios):

(1) Stop production and decay with 100% branching fraction to top plus neutralino. The decay is carried out using phase space alone, so the decay products are completely unpolarized. This setup is exactly the CMS simplified model T2tt [108].
(2) Right-handed stop production followed by decay to a binolike LSP plus a top quark. In practice we take the exact setup for scenario I but swap the roles of μ and M_1. This spectrum is close to the default signal model used by ATLAS. As the handedness of the stop and the identity of the LSP are fixed, the polarization of the emerging top quark is also fixed.

By comparing our scenarios with the stop signal models usually used, we can see how the Higgsino-like nature of the LSP and the hierarchy of the third-generation squarks affects what regions of parameter space are allowed. The comparisons also give some indication of how well our simple analysis matches the full ATLAS/CMS results.

We can understand the strength of the bounds on our scenarios by looking at the branching ratios and final states of our spectra. As we have decoupled the gauginos in all of our setups, the decays of the stops and sbottoms are governed entirely by the Yukawa couplings. For example, in scenario I, all decays come from the top Yukawa; up to kinematics, this yields a 50-50 split between decays to top quark plus neutralino and bottom quark plus chargino.[6] Due to the degeneracy of the chargino-neutralino sector, chargino decay products are all extremely soft. In particular, the leptons from a chargino decay are far too soft to trigger the analysis requirements for the stop analysis; thus, the only source of leptons is from the stops that decay to a leptonically decaying top quark. Additionally, mixed decays $\tilde{t}_1\tilde{t}_1^* \to t(\to \ell\nu b) + \tilde{\chi}^0 + b + \tilde{\chi}_1^\pm$ may have a hard lepton, but they typically have fewer jets than required for a stop analysis. Therefore, only the fraction of events where both the stop and antistop decay to top + neutralino have a high probability of passing the analysis requirements. As a final suppression, because the light stop in scenario I is (almost) entirely right handed, the top quarks it yields are left-handed. Due to the V-A nature of the weak interaction, left-handed tops have a softer lepton spectrum, and thus the leptons that the stops decays do create are less likely to pass the analysis cuts [128]. The combined effect of these suppression factors is that there is no bound from the CMS direct stop search on scenario I.

Similar logic works to understand the bounds on scenarios II and III. In scenario II, both the b_L and t_L are produced. Up to effects of $O(y_b \tan\beta)$ and ignoring

[5]For example, in scenario III the spectrum also contains a second stop and a sbottom—all three states are produced and analyzed when deriving the analysis efficiencies, though limits are still placed in terms of the lightest stop eigenstate.

[6]The neutralino branching fraction is further split: roughly 50% to $\tilde{\chi}_1^0$ and 50% to $\tilde{\chi}_2^0$. However, this distinction does not affect our analysis since the two states have essentially the same mass.

kinematics, the only decay channel possible is $\tilde{t} \to t + \tilde{\chi}^0$ for the stop and $\tilde{b} \to t + \tilde{\chi}_1^-$ for the sbottom. The stop therefore decays in exactly the same way as in the default scenario, so we expect the bound to be at least as strong as the T2tt bound (with the added effect that the top is always right-handed, and thus the emitted lepton is harder than in the unpolarized case). The bound is actually stronger because the sbottom decays also contribute; the chargino in a sbottom decay is indistinguishable from a neutralino, so the final state from a sbottom decay is virtually identical to the stop case. The only place the bound on scenario II may weaken is close to or below the $t + \tilde{\chi}^0$ threshold, where $\tilde{t} \to b + \tilde{\chi}_1^+$ decays become important. Finally, we expect an even stronger bound in scenario III. In addition to the $\tilde{b}$ decay that contributes exactly as in scenario III, there are now two stop states, and both states will contribute to the stop search. These suspicions are confirmed in Fig. 2.

Moving to the ATLAS semileptonic stop search, we find similar results, shown in Fig. 3. This is not surprising as the search criteria are very similar to the CMS stop search—a single hard lepton and four or more hard jets. The biggest difference between the ATLAS and CMS semileptonic stop searches is that ATLAS requires a "hadronic top candidate"—a three-jet subsystem with mass between 130 GeV and 205 GeV—in all events. This requirement, along with slight changes in the analysis variables (see Appendix B), lead to different limits, but the qualitative message is the same as in the previous case: scenarios with $m_{\tilde{t}_R} \ll m_{\tilde{t}_L}, m_{\tilde{b}_L}$ are not bounded by these searches because the stops decay preferentially to $b + \tilde{\chi}_1^\pm$ and therefore lack sufficient hard leptons and jet multiplicity, while scenarios with light $\tilde{t}_L$, $\tilde{b}_L$ are bounded tighter than the benchmark $\tilde{t} \to t + \tilde{\chi}^0$ scenario because both the stop and the sbottom decays contain top quarks.[7]

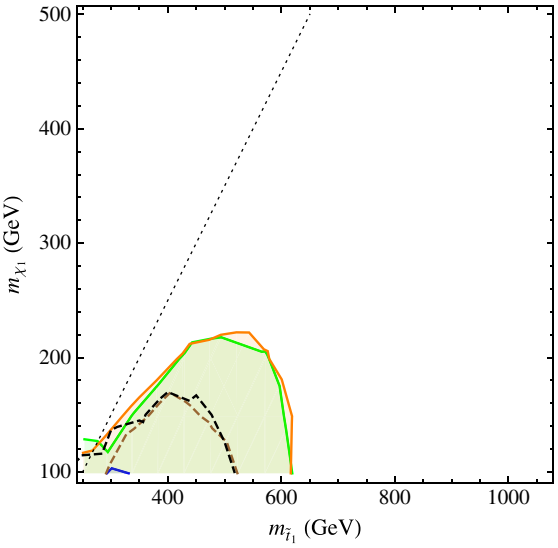

FIG. 3 (color online). Limits on the various third-generation scenarios coming from the ATLAS direct stop search (semileptonic channel). Contours are the same as in Fig. 2.

The final direct-stop analysis we explore is an all-hadronic search performed by ATLAS using 20.5 fb^{-1} of data.[8] Unlike the previous stop analysis, no leptons are involved. Instead, stops are searched for in events with multiple hard jets (6 or more), at least two b jets, and substantial missing energy. To suppress multijet QCD backgrounds, the jets in the event are required to form two top candidates—three-jet subsystems with invariant mass between 80 and 270 GeV. When interpreted in terms of the $\tilde{t}_1 \to t + \tilde{\chi}^0$ benchmark scenario, ATLAS finds the strongest stop bound to date, nearly 700 GeV for the massless neutralino.

Applying these analyses to our three scenarios, the bounds we find are shown below in Fig. 4. The trend of these bounds is similar to what we found in the previous stop searches, though the reasoning is slightly different. The bounds on scenarios II and III are nearly identical and rule out stops below 750 GeV for $\mu = 100$ GeV. There is no significant bound on scenario I due to the high fraction of decays to $b + \tilde{\chi}_1^\pm$; stop decays to bottom quarks do not contain enough hadronic activity to efficiently pass the jet multiplicity cuts in this analysis.

Summarizing the direct stop searches, scenarios with degenerate, light Higgsinos and $\tilde{t}_R \ll \tilde{t}_L$, $\tilde{b}_L$ are very

[7]Comparing our bounds for $\tilde{t}_1 \to t\tilde{\chi}^0$ (T2tt model) with the exclusions from ATLAS, we see a discrepancy—our bounds are weaker by $O(100)$ GeV. The fact that the DELPHES-based bound is different from the quoted number is not surprising, but the discrepancy is somewhat larger than expected. ATLAS has provided a cut flow, at least for some benchmark $(m_{\tilde{t}_1}, m_{\tilde{\chi}_1^0})$ points, which allows us to pinpoint the difference to the m_{jjj} cut [relative efficiencies of cuts either before or after this cut match to $O(10\%)$]. We suspect the reason the m_{jjj} cut is discrepant is that the jet-energy resolution in DELPHES is overly optimistic. If the jets retain too much of their energy, then the m_{jjj} distribution will be shifted to higher values (relative to the full detector) and lost once the cut $m_{jjj} < 205$ GeV is imposed. If we increase the upper m_{jjj} cut by ~50 GeV, the signal efficiency at the benchmark point agrees better with the quoted value; however, this artificial shift will have uncontrollable implications in the rest of the $(m_{\tilde{t}_1}, m_{\tilde{\chi}_1^0})$ efficiency plane. Therefore, we stay with the quoted cuts and emphasize that the relative bounds between models are the most relevant. The strong sensitivity of the bounds to m_{jjj} also serves as a warning to the experiments since m_{jjj} is susceptible to effects from ISR, the underlying event, and pileup.

[8]ATLAS has performed a stop search in the dilepton final state [129] assuming BR$[\tilde{t}_1 \to b\chi^\pm] \sim 100\%$ and using a variety of chargino-neutralino mass splittings (though none consistent with $\mu \ll M_1, M_2$). As the search requires two leptons, the same issues raised for scenario I will be present, and we expect no bound. For scenarios II and III, we expect stronger limits from the semileptonic search since the decay $\tilde{t}_1 \to t\tilde{\chi}_0^0$ is dominant. For these reasons we do not explore the limits from the dileptonic searches on natural supersymmetry.

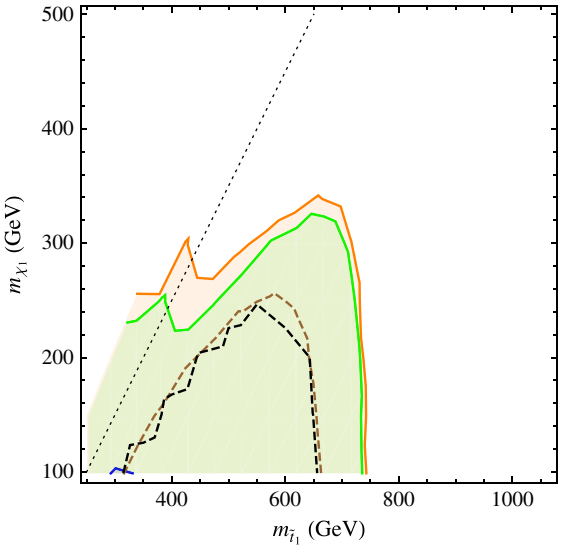

FIG. 4 (color online). Limits on the various third-generation scenarios coming from the ATLAS direct stop search (all-hadronic channel). Contours are the same as in Fig. 2.

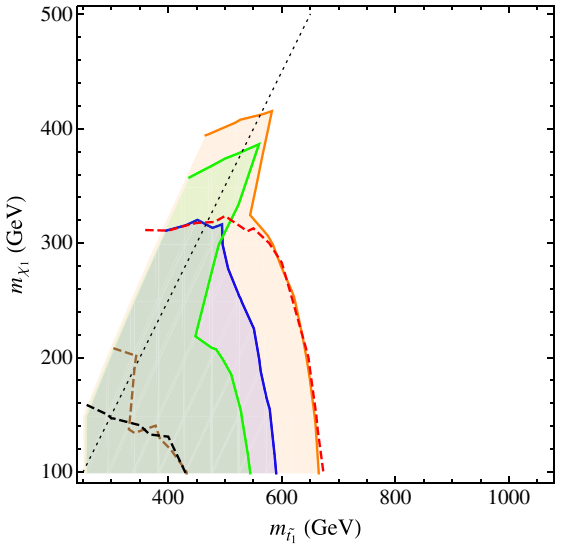

FIG. 5 (color online). Limits on our third-generation scenarios from the CMS direct sbottom search. Contours are the same as in Fig. 2: identifying the contours by the highest exclusion in $m_{\tilde{\chi}_0}$, the highest solid contour (orange) shows the 95% exclusion bound on scenario III, the second highest solid contour (green) shows the 95% exclusion bound on scenario II, and the lowest solid contour (blue) shows the 95% exclusion bound on scenario I. Notice that the bound on scenario I extends to higher $m_{\tilde{t}_1}$ mass than scenario II at lower $m_{\tilde{\chi}_1}$ masses. We have also added the bound (red dashed line) derived from applying this analysis to the T2bb simplified model, direct production of right-handed sbottoms with 100% branching fraction to a bottom quark and a neutralino. The remaining contours are the same as in Fig. 2.

weakly bounded, while the bounds on scenarios with light $\tilde{t}_L$, $\tilde{b}_L$ are quite tight, typically 100 GeV stronger than the bounds on the benchmark $\tilde{t}_1 \to t + \tilde{\chi}^0$ setup. Because the direct stop searches are so insensitive to light $\tilde{t}_R$ (with light μ), the bounds on scenario II ($\tilde{t}_L$, $\tilde{b}_L$ and $\tilde{t}_R$ all light) and scenario III (only t_L, b_L light) are nearly identical. However, before we can draw any firm conclusions on natural supersymmetry, we must also consider the CMS and ATLAS searches tailored toward the detection of sbottoms.

C. Direct sbottom searches

In natural supersymmetry, the stops can decay into $b + \tilde{\chi}_1^{\pm}$, and thus dedicated searches for b quarks plus missing energy are vital to our analysis. In addition, in both scenarios II and III, $\tilde{b}_L$ is present in the spectrum with $m_{\tilde{b}_L} \simeq m_{\tilde{t}_L}$ determined by m_{Q_3}. In this section we use the ATLAS and CMS searches that target direct sbottoms [44,45], since these studies focus on b jets and missing energy and are therefore independent of the mass splittings in the chargino/neutralino sector.

To isolate signal-rich regions from background, ATLAS/CMS sbottom searches require multiple high-p_T jets along with one or more flavor tags. Events with leptons are vetoed as a way to remove some $\bar{t}t$ background (the leptonic events are retained as control samples). More elaborate cuts are applied to further enhance the signal depending on the collaboration and the target signal mass. The default signal we will compare to is pair production of sbottoms that decay solely to b quarks plus a neutralino, a $\bar{b}b + \not{E}_T$ final state. Since it is identical to the CMS default signal model, we will refer to the default as T2bb as they do.

To bound $\bar{b}b + \not{E}_T$ signals, CMS [45] retains events with 2–3 jets and 1 or 2 b tags. The visible objects in the event are partitioned into two "megajets." The degree to which these megajets balance each other, described with the α_T variable [130,131], as well as the net H_T are used to further isolate the signal from background. The bounds from this analysis on the CMS default model and on our three scenarios are shown below in Fig. 5.

The first thing to notice is that the sbottom search places a strong bound on scenario I—roughly $m_{\tilde{t}_1} > 600$ GeV for $m_{\tilde{\chi}_1^0} \sim \mu \sim 100$ GeV and decreasing slightly as $m_{\tilde{\chi}_1^0}$ is raised.

The bounds on scenario I are weaker than the bounds on the T2bb scenario. This is because scenario I yields more leptons—coming, as before, from stop decays to leptonic tops—so events from scenario I are more likely to be vetoed. Also, the average number of jets is higher, pushing the signal into jet bins not considered in the sbottom analysis. The same two effects also explain the difference in bounds between scenarios I and II. In scenario II, provided $m_{\tilde{t}_1} \gg m_t + m_{\tilde{\chi}_1^0}$, both stop and sbottom decays result in top quarks. The only ditop quark events that cleanly mock the $\bar{b}b + \not{E}_T$ signal are fully leptonic events where both leptons are lost or lie outside the tracking volume. In all

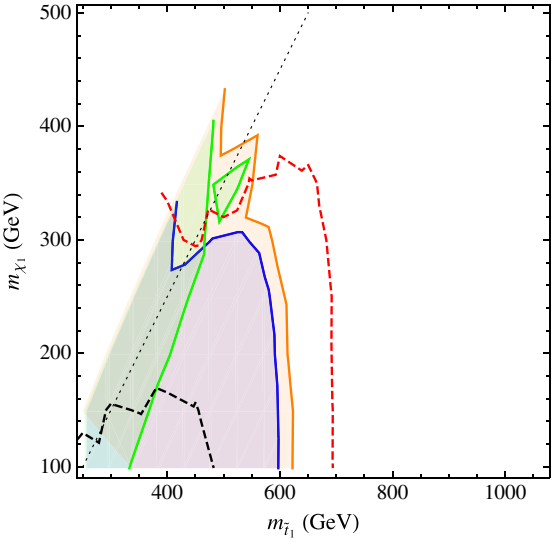

FIG. 6 (color online). Limits on our third-generation scenarios from the ATLAS direct sbottom search. Contours are the same as in Fig. 5.

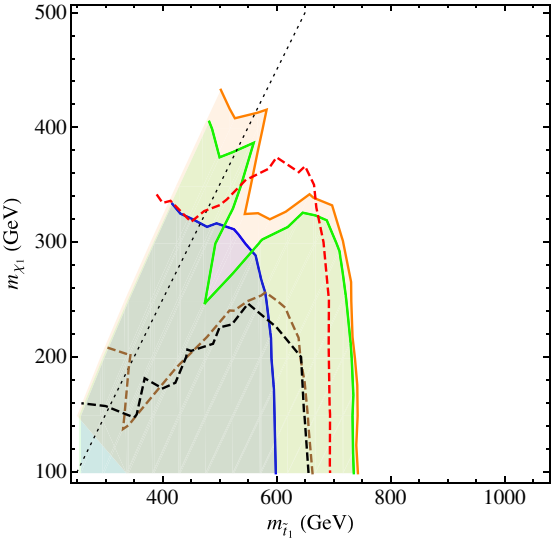

FIG. 7 (color online). Limits on our third-generation scenarios from combining all CMS and ATLAS sbottom/stop searches search. Contours are the same as in Fig. 5.

other events there is either a lepton or a larger jet multiplicity, and the event is either vetoed or populates a region not usually considered as signal. The caveat to this argument is when $m_{\tilde{t}_1} \lesssim m_t + m_{\tilde{\chi}_1^0}$. In this region, kinematics suppresses the $\tilde{t}_1 \to t + \tilde{\chi}^0$ mode, and the (otherwise Yukawa suppressed) $\tilde{t}_1 \to b + \tilde{\chi}_1^\pm$ mode becomes important. Decays to $b + \tilde{\chi}_1^\pm$ are efficiently selected by the CMS search, explaining why the bound on scenario II gets stronger the closer the stop mass gets to $m_t + m_{\tilde{\chi}_1^0}$. The bound in the threshold region of scenario II is actually stronger than in scenario I since both $\tilde{t}_L$ and $\tilde{b}_L$ are produced and both decay to $b + \tilde{\chi}$ when $m_{\tilde{t}_1} \sim m_{\tilde{b}_1} \lesssim m_t + m_{\tilde{\chi}^0}$. As expected, the bound on scenario III is the strongest and resembles the sum of the bounds on scenarios I and II.

The ATLAS direct sbottom [44] search targets the same final state, $\bar{b}b + \not{E}_T$, as the CMS search. However, the ATLAS search is more optimized to the topology with exactly two bottom jets, missing energy, and little other hadronic activity. A third hard jet is vetoed in the majority of the analysis channels, and no channel tolerates 4 or more jets. As a result, the ATLAS sbottom search is less flexible and not as well suited to events that contain top quarks. The bounds from the ATLAS sbottom search cast in terms of our scenarios and the benchmark T2bb model are shown below in Fig. 6.[9]

[9]In the ATLAS analysis [132], the sbottom search technique was used to constrain stop production, exactly as we are advocating here. However, in that analysis, $\mathrm{BR}(\tilde{t}_t \to b\tilde{\chi}_1^\pm) = 1$ was assumed, so bounds presented there do not constrain scenarios with a light Higgsino, a key ingredient in natural supersymmetry.

D. Combined bounds

Combining the three stop searches and two sbottom searches by taking the strongest limit at a given $(m_{\tilde{t}_1}, m_{\tilde{\chi}_1^0})$ point, we get the net excluded region for the three scenarios. The excluded regions are displayed below in Fig. 7 along with the analogous regions for the default spectra.

IV. IMPLICATIONS FOR THE HIGGS SECTOR

In this section we study the implications of scenarios I, II, and III on the supersymmetric Higgs sector. In supersymmetry the additional charged and colored degrees of freedom can significantly modify the production cross section and branching ratios of the lightest (standard model-like) Higgs boson [92–105]. Given the recent discovery of a particle consistent with a Higgs boson at $m_h \simeq 125$ GeV [77,78], the modifications due to the additional charged and colored degrees of freedom have been extensively studied [40,82–88,90,91,133].

First let us consider the Higgs boson branching ratios. When the stop contributions are included, the modification to the decay rate of the Higgs boson into gluons is given by [102,134]

$$\frac{\Gamma_{ggh}^{\mathrm{MSSM}}}{\Gamma_{ggh}^{\mathrm{SM}}} \simeq \left| 1 + \frac{1}{A_{1/2}(\tau_t)} \sum_{i=1}^{2} \frac{g_{h\tilde{t}_i\tilde{t}_i}}{m_{\tilde{t}_i}^2} A_0(\tau_{\tilde{t}_i}) + \frac{1}{A_{1/2}(\tau_t)} \sum_{i=1}^{2} \frac{g_{h\tilde{b}_i\tilde{b}_i}}{m_{\tilde{b}_i}^2} A_0(\tau_{\tilde{b}_i}) \right|^2, \quad (17)$$

where $A_{1/2}(A_0)$ are the standard fermion (scalar) loop functions (e.g., Ref. [134]), and $\tau_i = m_h^2/4m_i^2$. Here $m_{\tilde{f}_2} \geq m_{\tilde{f}_1}$, θ_f is the sfermion the mixing angle, and the couplings are given by

$$\frac{g_{h\tilde{f}_i\tilde{f}_i}}{m^2_{\tilde{f}_i}} \simeq \frac{m^2_f}{m^2_{\tilde{f}_i}} + \frac{(-1)^i}{4} s^2_{2\theta_f} \frac{m^2_{\tilde{f}_2} - m^2_{\tilde{f}_1}}{m^2_{\tilde{f}_i}} + \mathcal{O}\left(\frac{M^2_Z}{m^2_{\tilde{f}_i}}\right) \quad (18)$$

in the decoupling limit. Hence, in the limit of small mixing, $\theta_f \sim 0$, the squarks enhance the decay rate of the Higgs boson into gluons. Similarly, for sbottoms the contributions are typically small except in the large tan β regime where sbottom contributions will interfere destructively with the top contribution.

Light stops, sbottoms, staus, and charginos also affect the decay of the Higgs boson into photons. Enhancing the decay rate of the Higgs to gluons due to light stops will lead to a suppressed decay rate of the Higgs into photons due to the stop contribution destructively interfering with the W-boson contribution (the dominant standard model

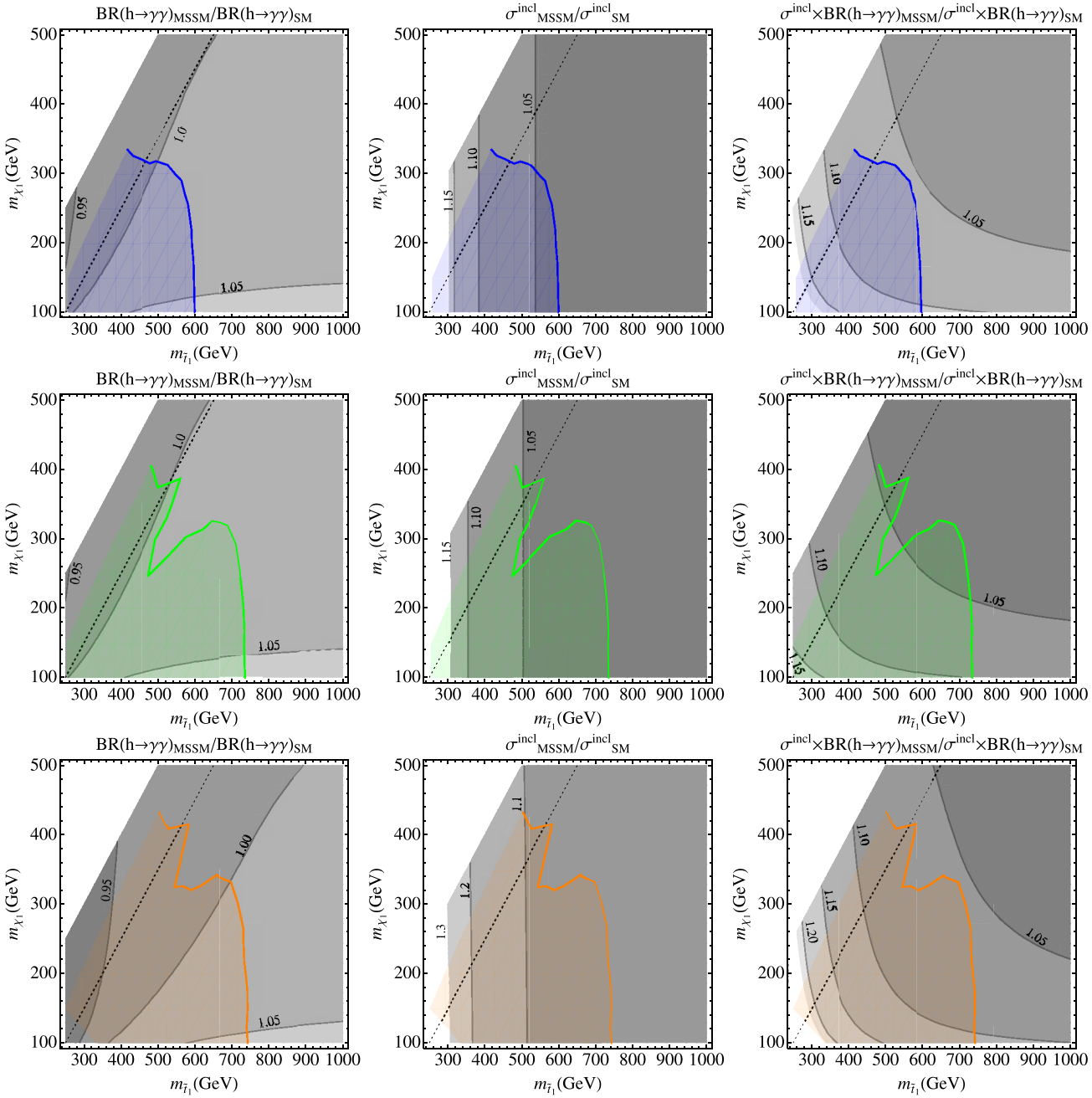

FIG. 8 (color online). Modifications to Higgs production and branching ratios in the decoupling limit where $M_A \to \infty$, $A_t = A_b = 0$ and $M_2 = 1$ TeV. We have overlain the direct search constraints found in Fig. 7 (same coloring). The top, middle, and lower set of figures correspond to scenarios I, II, and III. The compressed wedge corresponds to the allowed region in the upper left of each plot, where the mass difference between the squark and the Higgsinos is small. The kinematic limit region corresponds to the allowed region to the far right of each plot, where the squark production cross section reaches the kinematic limit of the LHC searches.

contribution), while a light sbottom has the opposite effect. Furthermore, depending on the sign of μ, a light Higgsino close to the LEP bound [135] can either enhance or suppress the photon rate [136]. Expanding in terms of the $1/M_2$, where M_2 is the wino mass parameter, we find the amplitude of the lightest chargino is

$$|A_{\tilde{\chi}^\pm}| \approx \frac{2M_W^2}{|M_2| m_{\tilde{\chi}_1^0}} |c_{\alpha+\beta}| A_{1/2}(\tau_{\tilde{\chi}_1^0}), \tag{19}$$

where M_W is the W-boson mass, M_2 is the wino mass, $m_{\tilde{\chi}_1^0} \sim \mu$ and α is the mixing angle of the CP-even Higgs bosons. In the decoupling limit $c_{\alpha+\beta} \sim s_{2\beta}$, this contribution becomes suppressed for large $\tan\beta$ [136]. Therefore, the charged contributions are also relatively suppressed in an MSSM-like framework.

In Fig. 8 we show the impact of the spectra in scenarios I, II, and III on modifications to $\mathrm{BR}(h \to \gamma\gamma)$, σ_{incl}, and $\sigma_{\mathrm{incl}} \times \mathrm{BR}(h \to \gamma\gamma)$. This is the principle result of our paper. We have taken $\mu > 0$ and $M_A = \infty$; however the results are nearly identical (to within $\simeq$5%) when $M_A = 1000$ GeV.[10] Here we have assumed there is an additional contribution to the quartic coupling, raising the Higgs mass up to the experimentally measured value $m_h \simeq 125$ GeV, such as the NMSSM-like scenario described in Appendix A.

We see that the modifications to the inclusive production cross section (dominated by gluon fusion) are at the 10–30% level in the compressed wedge, while rather small $\lesssim 5\%$ at the kinematic limit. The $\mathrm{BR}(h \to \gamma\gamma)$ receives considerably smaller effects, between -5% to $+5\%$ across the parameter space of interest. These deviations are not large enough to be directly constrained by the measurements from the LHC [137] and Tevatron [138]; however, as we measure the Higgs production and branching ratios more precisely, we expect these deviations to be observable at the LHC.

V. DISCUSSION

We have shown that natural supersymmetry, where third-generation squarks decay into Higgsino-like neutralinos and chargino, is significantly constrained by existing LHC searches, summarized in Fig. 7. When these constraints are overlaid on the modifications to the lightest Higgs production and decay, shown in Fig. 8, we find distinctly different implications for the remaining allowed regions identified as the compressed wedge $[(m_{\tilde{q}} - |\mu|)/m_{\tilde{q}} \ll 1)]$ and the kinematic limit ($m_{\tilde{q}} >$ 600–750 GeV). We found that the collider constraints arise from the totality of numerous searches at ATLAS and CMS that are separately sensitive, in varying degrees, to squark production and decay through $\tilde{t} \to t\tilde{\chi}^0$, $\tilde{t} \to b\tilde{\chi}_1^+$, $\tilde{b} \to b\tilde{\chi}^0$, and $\tilde{b} \to t\tilde{\chi}_1^-$. Our analysis incorporated simulations of the signal and detector response, matching the experimental analyses as close as we could. Nevertheless, there is substantial room for improvement. Much of the experimental searches were designed for only one decay mode, or chose chargino/neutralino mass hierarchies that are not consistent with natural supersymmetry. We believe dedicated analyses, that take into account the proper branching fractions and mass hierarchy, may well significantly improve the sensitivity.

Natural supersymmetry implies the wino and bino are sufficiently heavy that the Higgsino-like chargino and neutralino splittings are very small, just several GeV. While we focused our attention on the stop/sbottom signals, the electroweakinos (Higgsinos) can be directly produced at the LHC. However, the narrow splittings of the Higgsinos make them extremely difficult to detect; the traditional search for electroweakinos is $pp \to \tilde{\chi}_2^0 \tilde{\chi}_1^\pm \to 3\ell + \not{E}_T$ [139], where the leptons come from cascade decays $\tilde{\chi}_2^0 \to Z\tilde{\chi}_1^0$, $\tilde{\chi}_1^\pm \to W^\pm \tilde{\chi}_1^0$. As the spectrum gets squeezed, the intermediate $W^\pm/Z^0$ go off shell, and the leptons they decay to are too soft to pass analysis cuts. Current searches are restricted to on-shell $W^\pm/Z^0$, so there is no bound from trilepton searches on degenerate Higgsinos. Exactly what $m_{\tilde{\chi}_2^0} - m_{\tilde{\chi}_1^0}$, $m_{\tilde{\chi}_1^\pm} - m_{\tilde{\chi}_1^0}$ mass splitting the experiments are sensitive to is a very interesting question, but beyond the scope of this paper.

A more promising way to detect degenerate Higgsinos may be through monojet searches [140]. The initial quark/antiquark in $q\bar{q} \to \tilde{\chi}\,\tilde{\chi}$ production can emit hard radiation that recoils against the invisible portion of the event. Current monojet searches look for, among other physics, dark matter production after pairs of dark matter particles escape the detector. Reinterpreting the monojet bounds in terms of Higgsino pair production, we estimate that the current searches are sensitive to $\mu \sim 100$ GeV [141], competitive with the LEP bound on charginos [135]. With more data, this bound may increase, slicing into the parameter space of natural supersymmetry. Additionally, there may be methods to optimize monojet searches for Higgsinos; the existing searches assume higher-dimensional contact operators whereas Higgsinos couple directly through electroweak gauge bosons.

If the natural supersymmetry expectations for M_2, M_1 are relaxed, it is also interesting to investigate how sensitive the LHC will be to stop and sbottoms with light Higgsinos. Two effects arise from lowering M_2 and/or M_1: the splittings between the Higgsinos increase, and the gaugino content of the lightest electroweakinos increases. Since stop and sbottom decays to Higgsino-like electroweakinos are dominated by the top Yukawa coupling, we do not anticipate significant effects on the decay branching fractions even when $M_{2,1}$ drop below $m_{\tilde{q}}$, opening up decays to gauginos. The larger effect is the

[10]For lower values of m_A, the increased mixing between the two CP-even Higgs bosons leads to a slight further suppression in the branching ratios.

increase in the splittings between the Higgsinos themselves. Clearly another interesting question is to probe how large the splitting needs to be before the search strategies described here become diluted by the additional energy from transitions between Higgsinos. Mixing the light electroweakinos with some bino, wino, or singlino is highly relevant for the possibility that the lightest neutralino could be dark matter, but this is beyond the scope of this paper.

Natural supersymmetry may also lead to an unusual signal for the first- and second-generation squarks. One decay possibility for a first-/second-generation squark in natural supersymmetry is to a quark plus a Higgsino. As the first- and second-generation Yukawas are so small, the decay proceeds through the wino/bino fraction of the lightest neutralino and is therefore suppressed by $O(gv^2/M_{1,2})$. A second decay possibility is the three-body decay, $\tilde{q} \to j + \tilde{t}_1 t$ or $j + \tilde{b}_1 b$ via an off-shell gluino. This option is suppressed by the gluino mass and three-body phase space but comes with QCD coupling strength. Depending on the hierarchy of M_3, M_2 as well as the mass of the light squarks relative to the stops/sbottoms, the three-body decay fraction can be substantial.[11] First-/second-generation squark decays to $j\tilde{t}_1 t$ or $j\tilde{b}_1 b$ would have several consequences that would be interesting to explore in more detail. Two obvious consequences are that the energy per final state particle would be lower because the squarks decay to multiple particles, and the decays would contain heavy-flavor jets not usually associated with first-/second-generation searches.

Finally, while natural supersymmetry in a low-energy effective theory is straightforward to define and quantify, issues of naturalness become muddled as this is embedded into an ultraviolet completion. The obvious issue is the that leading-log corrections to the electroweak symmetry breaking scale can quickly become a poor approximation if the renormalization group evolution is substantial. For instance, ''radiative'' electroweak symmetry breaking arises when $m_{H_u}^2$ is ''driven'' negative by its interaction with the stops, which clearly requires renormalization group improvement to determine the size of the contribution to electroweak symmetry breaking. This is precisely why we considered $m_{\tilde{q}}$ and μ to be free parameters, since their separation may be much smaller than the leading-log approximation suggests. How this impacts the larger spectrum, particularly the gluino, becomes a highly model-dependent question. Nevertheless, we believe our analysis has captured the essential physics of natural supersymmetry, and we remain optimistic that it can be discovered with continued analyses at the LHC.

[11]The strength of the three-body mode also depends on the mass character of the gluino. For Dirac gluinos the suppression in the three-body mode is $m_{\tilde{q}}/M_3^2$ rather than $1/M_3$, making it much smaller.

ACKNOWLEDGMENTS

We thank Nima Arkani-Hamed, Mariangela Lisanti, Joe Lykken, Steve Martin, Steve Mrenna, and Gilad Perez for many valuable conversations. A. M. thanks Boston University for computing resources. G. D. K. thanks the Ambrose Monell Foundation for support while at the Institute for Advanced Study. G. D. K. and A. M. are supported in part by the US Department of Energy under Contract No. DE-FG02-96ER40969.

APPENDIX A: REALIZING THE OBSERVED HIGGS MASS AND BRANCHING RATIOS OF SCENARIOS I, II, AND III

In this appendix, we consider the possibility of realizing natural supersymmetry scenarios with $m_h \sim 125$ GeV. In particular we consider the NMSSM model [142] where the Higgs sector of the MSSM is extended by including a gauge singlet. The superpotential has the form

$$W = W_{\rm Yuk} + \lambda \hat{H}_u \hat{H}_d \hat{S} + \frac{\kappa}{3}\hat{S}^3, \tag{A1}$$

where $W_{\rm Yuk}$ are the usual Yukawa interactions and the hatted fields denote the chiral superfields. The corresponding soft supersymmetry breaking terms are

$$V_{\rm soft} = m_{H_u}^2 |H_u|^2 + m_{H_d}^2 |H_d|^2 + m_S^2 |S|^2 + \lambda A_\lambda S H_u H_d + \frac{\kappa A_\kappa}{3} S^3. \tag{A2}$$

In addition to the D-term contributions to the Higgs mass, the additional $\lambda v^2 \sin^2 2\beta$ contribution can help raise the Higgs mass above the Z-boson mass. On the other hand, solving the minimization conditions leads to the electroweak symmetry breaking condition of Eq. (1) with $\mu \to \lambda x$.[12] To maximize the tree-level contributions to the Higgs mass, we need both the NMSSM quartic contribution as well as the usual D-term contribution, and thus small $\tan\beta$. Small $\tan\beta$ typically enhances the hierarchy between m_{H_u}, m_{H_d} and the electroweak scale.[13] Due to this tension between the Higgs mass and the hierarchy of scales, we consider $\tan\beta \in (1.5, 2)$. However, we can still simultaneously realize the natural supersymmetry spectra in this paper and the observed Standard Model Higgs mass in the NMSSM. Using NMSSMtools3.2.4 [146], we find $m_h \simeq 125$ GeV for the parameter space point $\tan\beta = 1.5$, $A_t = A_b = A_\tau = 0$, $m_{\tilde{f}}^2 = 700$ GeV, $M_1 = M_2 = M_3 = 2$ TeV, $\lambda = 0.7$, $\kappa = 0.67$, $A_\lambda = -60$ GeV, $A_\kappa = -200$ GeV, and $\mu_{\rm eff} = 200$ GeV. Also, for this

[12]The additional minimization condition of the singlet leads to a modified fine-tuning condition for the NMSSM. A detailed discussion of the fine-tuning in the generalized NMSSM-like models can be found in Refs. [36,143,144].

[13]For alternative NMSSM scenarios using large $\tan\beta$, see Ref. [145].

parameter point, the low-energy precision and flavor observables are within 2σ of their experimental values.[14] For this point the neutralino masses are $m_{\tilde{\chi}^0} =$ (197 GeV, 227 GeV, 416 GeV, 1.98 TeV, 1.99 TeV), and the chargino masses are $m_{\tilde{\chi}^\pm} =$ (200 GeV, 1.98 TeV). We checked that the branching ratios of the squarks into Higgsinos are within 1–2% of the an MSSM model with similar sfermion and Higgsino masses.

APPENDIX B: SEARCH DETAILS

For completeness, in the following we detail the important search criteria for each collaboration's particular search strategy that was used in this paper.

1. CMS stops, semileptonic, 9.7 fb^{-1} [43]

Object identification:
(i) jets, $p_T > 30$ GeV, $|\eta_j| < 2.5$, anti-k$_T$, $R = 0.5$; flavor tagging applied to all jets within $|\eta_j| < 2.5$
(ii) electrons (muons), $p_T > 30$ GeV, $|\eta_\ell| < 1.44(2.1)$
(iii) Leptons within $\Delta R = 0.4$ of a jet are removed.

Basic cuts:
(i) $\not{E}_T > 50$ GeV
(ii) exactly 1 lepton passing the criteria above
(iii) 3 or more jets, with at least one b tagged.

Analysis:
(i) Events passing the basic selection cuts are binned according to the transverse mass of the MET + lepton system and the missing energy. Transverse mass is defined as

$$m^2_{T,\not{E}_T-\ell} = 2(\not{E}_T p_{T,\ell} - \vec{\not{p}}_T \cdot \vec{p}_{T,\ell}). \quad \text{(B1)}$$

(ii) The bins are, in the format $(m_{T,\min}, \not{E}_{T,\min})$, (150 GeV, 100 GeV), (120 GeV, 150 GeV), (120 GeV, 200 GeV), (120 GeV, 250 GeV), (120 GeV, 300 GeV), (120 GeV, 350 GeV), and (120 GeV, 400 GeV).
(iii) The bins are not exclusive, so the bin with the best limit at a given $(m_{\tilde{t}_1}, m_{\tilde{\chi}^0_1})$ point is used.

2. ATLAS stops, semileptonic, 20.7 fb^{-1} [41]

Object identification:
(i) jets, $p_T > 20$ GeV, $|\eta_j| < 2.5$, anti-k$_T$, $R = 0.4$; flavor tagging applied to all jets within $|\eta_j| < 2.5$
(ii) electrons (muons), $p_T > 10$ GeV, $|\eta_\ell| < 2.7(2.4)$
(iii) Any jet within $\Delta R = 0.2$ of an electron is removed.
(iv) Subsequently, any leptons within $\Delta R = 0.4$ of a jet are removed.

Basic cuts:
(i) exactly 1 lepton, which must have $p_{T,\ell} > 25$ GeV
(ii) 4 or more jets, at least one of which is b tagged; the four hardest jets must satisfy $p_T > 80$, 60, 40, and 25 GeV, respectively.

Analysis:
(i) Most channels require top reconstruction, done as follows: the closest pair of jets (in ΔR) that satisfy $m_{jj} > 60$ GeV are dubbed a "W-candidate." This candidate is combined with the nearest jet (again in ΔR). For the resulting three-jet system to be considered a successful top candidate, 130 GeV $< m_{jjj} <$ 205 GeV is required.
(ii) Other analysis cuts include the transverse mass of the $\not{E}_T - \ell$ system, the missing energy, the $\not{E}_T$ significance—defined as $\not{E}_T/\sqrt{H_{T,j_{1-4}}}$, and the $\Delta\phi$ between the missing energy (transverse) vector and the leading two jets.
(iii) In the channels designed to be sensitive to the highest stop masses, two other variables are included, $am_{T,2}$ and $m^\tau_{T,2}$, both of which are slight variants on the $m_{T,2}$ variable [148]. In $m_{T,2}$, as in these variations, the visible part of the event is divided into two, and all partitions of the missing energy are scanned over. The differences between $m_{T,2}$, $am_{T,2}$, and $m^\tau_{T,2}$ lie in whether all the visible particles are used or only some of them. In $am_{T,2}$, only the leading light jet, lepton, and highest weight b jet are taken as the visible part of the event, while in m^τ_{T2} only the leading lepton and leading light jet are used.
(iv) The channels dedicated to $\tilde{t} \to t + \tilde{\chi}^0$ are:
(1) One top candidate, alone with $\Delta\phi_{\not{E}_T - j_1} > 0.8$, $\Delta\phi_{\not{E}_T - j_2} > 0.8$, $\not{E}_T > 100$ GeV, $\not{E}_T$ signif. >13, $M_T > 60$ GeV. Events passing this selection are then separated into 12 finer bins according to their M_T and $\not{E}_T$:

$$M_T \in \{60\text{–}90 \text{ GeV}, 90\text{–}120 \text{ GeV}, 120\text{–}140 \text{ GeV}, >140 \text{ GeV}\}$$
$$\not{E}_T \in \{100\text{–}125 \text{ GeV}, 125\text{–}150 \text{ GeV}, >150 \text{ GeV}\}.$$

(2) One top candidate, along with $\Delta\phi_{\not{E}_T - j_2} > 0.8$, $\not{E}_T > 200$ GeV, $\not{E}_T$ signif. >13, $M_T >$ 140 GeV, $am_{T,2} > 170$ GeV.
(3) One top candidate, along with $\Delta\phi_{\not{E}_T - j_1} > 0.8$, $\Delta\phi_{\not{E}_T - j_2} > 0.8$, $\not{E}_T > 275$ GeV, $\not{E}_T$ signif. >11, $M_T > 200$ GeV, $am_{T,2} > 175$ GeV, $m^\tau_{T,2} > 80$ GeV.
(v) The analysis contains three channels aimed at the $\tilde{t} \to b + \tilde{\chi}^\pm$ final state. In these channels no top candidate is required. Instead there are stronger

[14] As λ and κ are both somewhat large, these couplings may develop a Landau pole before the grand unified theory scale. The UV completion of such models can be realized in "fat Higgs"-like scenarios [147]; however, a detailed study of this issue is beyond the scope of this paper.

requirements on the p_T and multiplicity of the b jets, and an additional cut on $m_{\rm eff}$, defined as the scalar sum of the p_T of all jets with $p_T > 30$ GeV summed together with the $\not{E}_T$ magnitude and $p_{T,\ell}$.

3. ATLAS stops, fully hadronic, 20.5 fb^{-1} [42]

Object identification:
(i) jets, $p_T > 20$ GeV, $|\eta_j| < 4.5$, anti-k$_T$, $R = 0.4$; flavor tagging applied to all jets within $|\eta_j| < 2.5$
(ii) electrons (muons), $p_T > 10$ GeV, $|\eta_\ell| < 2.7(2.4)$
(iii) Any jet within $\Delta R = 0.2$ of an electron is removed.
(iv) Subsequently, any leptons within $\Delta R = 0.4$ of a jet are removed.

Basic cuts:
(i) zero leptons passing the above criteria
(ii) $\not{E}_T > 130$ GeV
(iii) Six or more jets, where jets satisfy $p_T > 33$ GeV, $|\eta_j| < 2.8$; the leading two jets must have $p_T >$ 80 GeV, and at least two jets are b tagged.

Analysis:
(i) Two three-jet clusters are formed from the list of jets as follows: the three jets that are closest in the $\phi - \eta$ plane are taken as one such cluster, removed from the list, and then the process is repeated to extract the second group. The mass of these three-jet clusters is required to lie within 80 GeV $< m_{jjj} <$ 270 GeV in order to select events with two hadronic tops in the final state.
(ii) The transverse mass of the $\not{E}_T - b$ system, where the b closest in $\Delta\phi$ is used, is required to be $>$175 GeV to remove leptonic $\bar{t}t$ background.
(iii) $\Delta\phi_{\not{E}_T - j} > 0.2\pi$, where $\Delta\phi_{\not{E}_T j}$ is the angle between the missing energy vector and the closest jet. This cut is designed to remove backgrounds from mismeasured jets.
(iv) The remaining events are binned according to $\not{E}_T$: $\not{E}_T > 200$ GeV, $>$300 GeV and $\not{E}_T > 250$ GeV. Only the strongest limit at a given $(m_{\tilde{t}_1}, m_{\tilde{\chi}_1^0})$ point is used.

4. CMS sbottoms, multi-b + $\not{E}_T$, 11.7 fb^{-1} [45]

Object identification:
(i) jets, $p_T > 50$ GeV,[15] $|\eta_j| < 3.0$, anti-k$_T$, $R = 0.5$; flavor tagging applied to all jets within $|\eta_j| < 2.5$
(ii) electrons (muons), $p_T > 10$ GeV, $|\eta_\ell| < 2.4(2.1)$
(iii) Any jet within $\Delta R = 0.4$ of a lepton is removed.

Basic cuts:
(i) zero leptons
(ii) at least 2 jets; the hardest jet must lie within $|\eta| <$ 2.5, and the leading two jets must have $p_T >$ twice the nominal jet p_T requirement. Nominally this is $>$100 GeV, but for events with low-H_T, this cut may be softer. Events with high-p_T jets (i.e., passing nominal jet criteria) at $|\eta| > 3.0$ are vetoed.
(iii) $H_T > 275$ GeV, where H_T is the scalar sum of the p_T of all jets in the events.

Analysis cuts:
(i) All visible objects in the event are grouped into two megajets, following the criteria given in Ref. [131]. The degree to which the two megajets balance each other is captured by the variable $\alpha_T = \frac{E_{T,2}}{M_{T,jj}}$, the fraction of the transverse energy of the subleading (in p_T) megajet relative to the transverse mass of the megajet pair. Requiring $\alpha_T > 0.55$ greatly suppresses multijet QCD backgrounds.
(ii) Events surviving the α_T cut are categorized according to the jet and b-jet multiplicities, then binned in H_T.
(iii) The jet multiplicity categories are $N_{\rm jet} =$ 2–3, and $N_{\rm jet} = 4^+$. Within each jet multiplicity category, $N_b = 0$, 1, 2, 3, (4) is considered (obviously $N_b = 4$ is only considered in the $N_{\rm jet} >= 4$ class). For a given $(N_{\rm jet}, N_b)$, the H_T is binned as [275–325 GeV], [325–375 GeV], [375–475 GeV], [475–575 GeV], [575–675 GeV], [675–775 GeV], [775–875 GeV], and $>$875 GeV.[16]
(iv) For the direct sbottom search, only the $N_{\rm jet} =$ 2–3, $N_b = 0$, 1 categories are used to set limits. Since the H_T bins are orthogonal, all H_T bins across both categories are taken together to form a combined limit.

5. ATLAS sbottoms, multi-b + $\not{E}_T$, 12.8 fb^{-1} [44]

Object identification:
(i) jets, $p_T > 20$ GeV, $|\eta_j| < 2.8$, anti-k$_T$, $R = 0.4$; flavor tagging applied to all jets within $|\eta_j| < 2.5$
(ii) electrons (muons), $p_T > 10$ GeV, $|\eta_\ell| < 2.7(2.4)$
(iii) Any jet within $\Delta R = 0.2$ of an electron is removed.
(iv) Subsequently, any leptons within $\Delta R = 0.4$ of a jet are removed.

Basic cuts:
(i) zero leptons
(ii) two or more jets, with two or more b-tags
(iii) $\not{E}_T > 150$ GeV.

Analysis:
(i) After basic selection, three event categories are set up, each with slightly different requirements. The categories are not exclusive:
(1) leading jet $p_T > 150$ GeV, subleading jet $p_T >$ 50 GeV, no other jets with $p_T > 50$ GeV. Both the leading two jets must be tagged as b jets. To reduce multijet QCD, $\Delta\phi_{\not{E}_T - j_2} > 0.4$ and

[15]This requirement is scaled down to 37 GeV, or 43 GeV for events with low H_T.

[16]For the samples with the highest b multiplicity, only three h_T bins are used, [275–325 GeV], [325–375 GeV], and $>$375 GeV.

$\not{E}_T/m_{\rm eff} > 0.25$ are required. Here $m_{\rm eff}$ is the scalar sum of the missing energy and the p_T of the hardest three jets satisfying basic jet requirements (meaning they must be harder than 20 GeV only), $m_{\rm eff} = \not{E}_T + \sum_{i=1}^{3} p_{T,j_i}$. Within this category, events are further binned according to their contratransverse mass; see Ref. [149] for the definition.

(2) similar to category 1, but the p_T requirements are adjusted to >200 GeV, >60 GeV for the leading and subleading jets. The leading two jets still must be flavor tagged, and the $\Delta\phi_{\not{E}_T - j_2}$ and the $\not{E}_T/m_{\rm eff}$ are unchanged.

(3) More than two jets are required with the leading jet having $p_T > 130$ GeV. The two subleading jets must have $p_T > 30$ GeV but below 110 GeV. Unlike the previous categories, the first two categories, the leading jet is not required to be a b jet. Instead the leading jet must have light flavor (it is antitagged), while the subleading two jets must be tagged as b jets. The $\Delta\phi_{\not{E}_T - j_2}$ and the $\not{E}_T/m_{\rm eff}$ are unchanged, but there is an additional requirement that the scalar sum of the p_T of all jets beyond the leading three is small, <50 GeV. This category is divided into two subcategories with different $\not{E}_T$ and p_{T,j_1} requirements.

[1] R. Barbieri and G. F. Giudice, Nucl. Phys. **B306**, 63 (1988).
[2] B. de Carlos and J. A. Casas, Phys. Lett. B **309**, 320 (1993).
[3] G. W. Anderson and D. J. Castano, Phys. Lett. B **347**, 300 (1995).
[4] A. G. Cohen, D. B. Kaplan, and A. E. Nelson, Phys. Lett. B **388**, 588 (1996).
[5] P. Ciafaloni and A. Strumia, Nucl. Phys. **B494**, 41 (1997).
[6] G. Bhattacharyya and A. Romanino, Phys. Rev. D **55**, 7015 (1997).
[7] P. H. Chankowski, J. R. Ellis, and S. Pokorski, Phys. Lett. B **423**, 327 (1998).
[8] R. Barbieri and A. Strumia, Phys. Lett. B **433**, 63 (1998).
[9] G. L. Kane and S. F. King, Phys. Lett. B **451**, 113 (1999).
[10] L. Giusti, A. Romanino, and A. Strumia, Nucl. Phys. **B550**, 3 (1999).
[11] M. Bastero-Gil, G. L. Kane, and S. F. King, Phys. Lett. B **474**, 103 (2000).
[12] J. L. Feng, K. T. Matchev, and T. Moroi, Phys. Rev. Lett. **84**, 2322 (2000).
[13] A. Romanino and A. Strumia, Phys. Lett. B **487**, 165 (2000).
[14] J. L. Feng, K. T. Matchev, and T. Moroi, Phys. Rev. D **61**, 075005 (2000).
[15] Z. Chacko, Y. Nomura, and D. Tucker-Smith, Nucl. Phys. **B725**, 207 (2005).
[16] K. Choi, K. S. Jeong, T. Kobayashi, and K.-i. Okumura, Phys. Lett. B **633**, 355 (2006).
[17] Y. Nomura and B. Tweedie, Phys. Rev. D **72**, 015006 (2005).
[18] R. Kitano and Y. Nomura, Phys. Lett. B **631**, 58 (2005).
[19] Y. Nomura, D. Poland, and B. Tweedie, Nucl. Phys. **B745**, 29 (2006).
[20] O. Lebedev, H. P. Nilles, and M. Ratz, arXiv:hep-ph/0511320.
[21] R. Kitano and Y. Nomura, Phys. Rev. D **73**, 095004 (2006).
[22] B. C. Allanach, Phys. Lett. B **635**, 123 (2006).
[23] G. F. Giudice and R. Rattazzi, Nucl. Phys. **B757**, 19 (2006).
[24] M. Perelstein and C. Spethmann, J. High Energy Phys. 04 (2007) 070.
[25] B. C. Allanach, K. Cranmer, C. G. Lester, and A. M. Weber, J. High Energy Phys. 08 (2007) 023.
[26] M. E. Cabrera, J. A. Casas, and R. Ruiz de Austri, J. High Energy Phys. 03 (2009) 075.
[27] S. Cassel, D. M. Ghilencea, and G. G. Ross, Nucl. Phys. **B825**, 203 (2010).
[28] R. Barbieri and D. Pappadopulo, J. High Energy Phys. 10 (2009) 061.
[29] D. Horton and G. G. Ross, Nucl. Phys. **B830**, 221 (2010).
[30] T. Kobayashi, Y. Nakai, and R. Takahashi, J. High Energy Phys. 01 (2010) 003.
[31] P. Lodone, J. High Energy Phys. 05 (2010) 068.
[32] M. Asano, H. D. Kim, R. Kitano, and Y. Shimizu, J. High Energy Phys. 12 (2010) 019.
[33] A. Strumia, J. High Energy Phys. 04 (2011) 073.
[34] S. Cassel, D. M. Ghilencea, S. Kraml, A. Lessa, and G. G. Ross, J. High Energy Phys. 05 (2011) 120.
[35] K. Sakurai and K. Takayama, J. High Energy Phys. 12 (2011) 063.
[36] G. G. Ross and K. Schmidt-Hoberg, Nucl. Phys. **B862**, 710 (2012).
[37] M. Papucci, J. T. Ruderman, and A. Weiler, J. High Energy Phys. 09 (2012) 035.
[38] G. Larsen, Y. Nomura, and H. L. L. Roberts, J. High Energy Phys. 06 (2012) 032.
[39] H. Baer, V. Barger, P. Huang, and X. Tata, J. High Energy Phys. 05 (2012) 109.
[40] J. R. Espinosa, C. Grojean, V. Sanz, and M. Trott, J. High Energy Phys. 12 (2012) 077.
[41] ATLAS Collaboration, Report No. ATLAS-CONF-2013-037.
[42] ATLAS Collaboration, Report No. ATLAS-CONF-2013-024.
[43] CMS Collaboration, Report No. CMS-PAS-SUS-12-023.
[44] ATLAS Collaboration, Report No. ATLAS-CONF-2012-165.

[45] CMS Collaboration, arXiv:1303.2985.
[46] ATLAS Collaboration, Report No. ATLAS-CONF-2012-105.
[47] ATLAS Collaboration, Report No. ATLAS-CONF-2012-145.
[48] CMS Collaboration, Report No. CMS-PAS-SUS-13-007.
[49] CMS Collaboration, Report No. CMS-PAS-SUS-12-024.
[50] T. Plehn, M. Spannowsky, M. Takeuchi, and D. Zerwas, J. High Energy Phys. 10 (2010) 078.
[51] T. Plehn, M. Spannowsky, and M. Takeuchi, J. High Energy Phys. 05 (2011) 135.
[52] X.-J. Bi, Q.-S. Yan, and P.-F. Yin, Phys. Rev. D **85**, 035005 (2012).
[53] Y. Bai, H.-C. Cheng, J. Gallicchio, and J. Gu, J. High Energy Phys. 07 (2012) 110.
[54] H. M. Lee, V. Sanz, and M. Trott, J. High Energy Phys. 05 (2012) 139.
[55] T. Plehn, M. Spannowsky, and M. Takeuchi, J. High Energy Phys. 08 (2012) 091.
[56] D. S. M. Alves, M. R. Buckley, P. J. Fox, J. D. Lykken, and C.-T. Yu, Phys. Rev. D **87**, 035016 (2013).
[57] Z. Han, A. Katz, D. Krohn, and M. Reece, J. High Energy Phys. 08 (2012) 083.
[58] D. E. Kaplan, K. Rehermann, and D. Stolarski, J. High Energy Phys. 07 (2012) 119.
[59] C. Brust, A. Katz, and R. Sundrum, J. High Energy Phys. 08 (2012) 059.
[60] J. Cao, C. Han, L. Wu, J. M. Yang, and Y. Zhang, J. High Energy Phys. 11 (2012) 039.
[61] M. L. Graesser and J. Shelton, arXiv:1212.4495.
[62] S. E. Hedri, A. Hook, M. Jankowiak, and J. G. Wacker, arXiv:1302.1870.
[63] B. Dutta, T. Kamon, N. Kolev, K. Sinha, K. Wang, and S. Wu, Phys. Rev. D **87**, 095007 (2013).
[64] A. Chakraborty, D. K. Ghosh, D. Ghosh, and D. Sengupta, arXiv:1303.5776.
[65] Y. Bai, H.-C. Cheng, J. Gallicchio, and J. Gu, arXiv:1304.3148.
[66] Y. Okada, M. Yamaguchi, and T. Yanagida, Prog. Theor. Phys. **85**, 1 (1991).
[67] H. E. Haber and R. Hempfling, Phys. Rev. Lett. **66**, 1815 (1991).
[68] J. R. Ellis, G. Ridolfi, and F. Zwirner, Phys. Lett. B **257**, 83 (1991).
[69] R. Barbieri, M. Frigeni, and F. Caravaglios, Phys. Lett. B **258**, 167 (1991).
[70] J. A. Casas, J. R. Espinosa, M. Quiros, and A. Riotto, Nucl. Phys. **B436**, 3 (1995); **B439**, 466(E) (1995).
[71] M. S. Carena, J. R. Espinosa, M. Quiros, and C. E. M. Wagner, Phys. Lett. B **355**, 209 (1995).
[72] M. S. Carena, M. Quiros, and C. E. M. Wagner, Nucl. Phys. **B461**, 407 (1996).
[73] H. E. Haber, R. Hempfling, and A. H. Hoang, Z. Phys. C **75**, 539 (1997).
[74] S. Heinemeyer, W. Hollik, and G. Weiglein, Eur. Phys. J. C **9**, 343 (1999).
[75] M. S. Carena, H. E. Haber, S. Heinemeyer, W. Hollik, C. E. M. Wagner, and G. Weiglein, Nucl. Phys. **B580**, 29 (2000).
[76] S. P. Martin, Phys. Rev. D **67**, 095012 (2003).
[77] ATLAS Collaboration, Phys. Lett. B **716**, 1 (2012).
[78] CMS Collaboration, Phys. Lett. B **716**, 30 (2012).
[79] R. Essig, E. Izaguirre, J. Kaplan, and J. G. Wacker, J. High Energy Phys. 01 (2012) 074.
[80] C. Brust, A. Katz, S. Lawrence, and R. Sundrum, J. High Energy Phys. 03 (2012) 103.
[81] L. J. Hall, D. Pinner, and J. T. Ruderman, J. High Energy Phys. 04 (2012) 131.
[82] S. Heinemeyer, O. Stal, and G. Weiglein, Phys. Lett. B **710**, 201 (2012).
[83] A. Arbey, M. Battaglia, A. Djouadi, F. Mahmoudi, and J. Quevillon, Phys. Lett. B **708**, 162 (2012).
[84] P. Draper, P. Meade, M. Reece, and D. Shih, Phys. Rev. D **85**, 095007 (2012).
[85] M. Carena, S. Gori, N. R. Shah, and C. E. M. Wagner, J. High Energy Phys. 03 (2012) 014.
[86] U. Ellwanger, J. High Energy Phys. 03 (2012) 044.
[87] K. Blum, R. T. D'Agnolo, and J. Fan, J. High Energy Phys. 01 (2013) 057.
[88] M. R. Buckley and D. Hooper, Phys. Rev. D **86**, 075008 (2012).
[89] A. Delgado, G. F. Giudice, G. Isidori, M. Pierini, and A. Strumia, Eur. Phys. J. C **73**, 2370 (2013).
[90] M. Carena, S. Heinemeyer, O. Stal, C. E. M. Wagner, and G. Weiglein, arXiv:1302.7033.
[91] M. Carena, S. Gori, N. R. Shah, C. E. M. Wagner, and L.-T. Wang, arXiv:1303.4414.
[92] M. A. Shifman, A. I. Vainshtein, M. B. Voloshin, and V. I. Zakharov, Yad. Fiz. **30**, 1368 (1979) [Sov. J. Nucl. Phys. **30**, 711 (1979)].
[93] M. Spira, A. Djouadi, D. Graudenz, and P. M. Zerwas, Nucl. Phys. **B453**, 17 (1995).
[94] B. A. Kniehl and M. Spira, Z. Phys. C **69**, 77 (1995).
[95] B. Kileng, P. Osland, and P. N. Pandita, Z. Phys. C **71**, 87 (1996).
[96] G. L. Kane, G. D. Kribs, S. P. Martin, and J. D. Wells, Phys. Rev. D **53**, 213 (1996).
[97] S. Dawson, A. Djouadi, and M. Spira, Phys. Rev. Lett. **77**, 16 (1996).
[98] A. Djouadi, V. Driesen, W. Hollik, and J. I. Illana, Eur. Phys. J. C **1**, 149 (1998).
[99] A. Djouadi, Phys. Lett. B **435**, 101 (1998).
[100] G. Belanger, F. Boudjema, and K. Sridhar, Nucl. Phys. **B568**, 3 (2000).
[101] R. V. Harlander and M. Steinhauser, J. High Energy Phys. 09 (2004) 066.
[102] R. Dermisek and I. Low, Phys. Rev. D **77**, 035012 (2008).
[103] R. Bonciani, G. Degrassi, and A. Vicini, J. High Energy Phys. 11 (2007) 095.
[104] I. Low, R. Rattazzi, and A. Vichi, J. High Energy Phys. 04 (2010) 126.
[105] R. V. Harlander, F. Hofmann, and H. Mantler, J. High Energy Phys. 02 (2011) 055.
[106] M. Blanke, G. F. Giudice, P. Paradisi, G. Perez, and J. Zupan, J. High Energy Phys. 06 (2013) 022.
[107] R. Barbieri, D. Buttazzo, K. Kannike, F. Sala, and A. Tesi, Phys. Rev. D **87**, 115018 (2013).
[108] CMS Collaboration, arXiv:1301.2175.
[109] M. Heikinheimo, M. Kellerstein, and V. Sanz, J. High Energy Phys. 04 (2012) 043.
[110] G. D. Kribs and A. Martin, Phys. Rev. D **85**, 115014 (2012).

[111] K. Benakli, M. D. Goodsell, and F. Staub, J. High Energy Phys. 06 (2013) 073.
[112] S. P. Martin, in *Perspectives on Supersymmetry II*, Advanced Series on Directions in High Energy Physics Vol. 21, edited by G. L. Kane (World Scientific, Singapore, 1997), pp. 1–153.
[113] S. Dimopoulos and G. F. Giudice, Phys. Lett. B **357**, 573 (1995).
[114] T. Sjostrand, S. Mrenna, and P. Z. Skands, J. High Energy Phys. 05 (2006) 026.
[115] J. Pumplin, D. R. Stump, J. Huston, H. L. Lai, P. M. Nadolsky, and W. K. Tung, J. High Energy Phys. 07 (2002) 012.
[116] S. Mrenna (private communication).
[117] W. Beenakker, R. Hopker, M. Spira, and P. M. Zerwas, Nucl. Phys. **B492**, 51 (1997).
[118] W. Beenakker, M. Kramer, T. Plehn, M. Spira, and P. M. Zerwas, Nucl. Phys. **B515**, 3 (1998).
[119] A. Kulesza and L. Motyka, Phys. Rev. Lett. **102**, 111802 (2009).
[120] A. Kulesza and L. Motyka, Phys. Rev. D **80**, 095004 (2009).
[121] W. Beenakker, S. Brensing, M. Kramer, A. Kulesza, E. Laenen, and I. Niessen, J. High Energy Phys. 12 (2009) 041.
[122] W. Beenakker, S. Brensing, M. Kramer, A. Kulesza, E. Laenen, and I. Niessen, J. High Energy Phys. 08 (2010) 098.
[123] W. Beenakker, S. Brensing, M. nKramer, A. Kulesza, E. Laenen, L. Motyka, and I. Niessen, Int. J. Mod. Phys. A **26**, 2637 (2011).
[124] LHC SUSY cross section working group, https://twiki.cern.ch/twiki/bin/view/LHCPhysics/~SUSYCrossSections8TeVstopsbottom.
[125] S. Ovyn, X. Rouby, and V. Lemaitre, arXiv:0903.2225.
[126] J. Conway, Report No. CDF/PUB/STATISTICS/PUBLIC/6428; J. Conway and K. Maeshima, Report No. CDF/PUB/EXOTIC/PUBLIC/4476.
[127] K. Cranmer and I. Yavin, J. High Energy Phys. 04 (2011) 038.
[128] ATLAS Collaboration, Report No. ATLAS-CONF-2012-166.
[129] ATLAS Collaboration, Report No. ATLAS-CONF-2012-167.
[130] L. Randall and D. Tucker-Smith, Phys. Rev. Lett. **101**, 221803 (2008).
[131] CMS Collaboration, Phys. Rev. Lett. **107**, 221804 (2011).
[132] ATLAS Collaboration, Report No. ATLAS-CONF-2013-001.
[133] M. Carena, S. Gori, N. R. Shah, C. E. M. Wagner, and L.-T. Wang, J. High Energy Phys. 07 (2012) 175.
[134] A. Djouadi, Phys. Rep. **459**, 1 (2008).
[135] LEP 2 SUSY Working Group, ALEPH, DELPHI, L3, and OPAL experiments, Report No. LEPSUSYWG/01-03.1, http://lepsusy.web.cern.ch/lepsusy; LEP 2 SUSY Working Group, ALEPH, DELPHI, L3, and OPAL experiments, Report No. LEPSUSYWG/02-04.1, http://lepsusy.web.cern.ch/lepsusy.
[136] R. Huo, G. Lee, A. M. Thalapillil, and C. E. M. Wagner, Phys. Rev. D **87**, 055011 (2013).
[137] ATLAS Collaboration, Report No. ATLAS-CONF-2013-034; CMS Collaboration, Report No. CMS-PAS-HIG-13-005.
[138] T. Aaltonen *et al.* (CDF and D0 Collaborations), arXiv:1303.6346.
[139] ATLAS Collaboration, Report No. ATLAS-CONF-2013-035; CMS Collaboration, Report No. CMS-PAS-SUS-12-022; CDF Collaboration, Report No. CDF/PUB/EXOTIC/PUBLIC/9817; V. M. Abazov *et al.* (D0 Collaboration), Phys. Rev. Lett. **95**, 151805 (2005).
[140] ATLAS Collaboration, Report No. ATLAS-CONF-2012-147; CMS Collaboration, Report No. CMS-PAS-EXO-12-048.
[141] G. Kribs, A. Martin, and A. Menon (to be published).
[142] P. Fayet, Nucl. Phys. **B90**, 104 (1975).
[143] U. Ellwanger, G. Espitalier-Noel, and C. Hugonie, J. High Energy Phys. 09 (2011) 105.
[144] G. G. Ross, K. Schmidt-Hoberg, and F. Staub, J. High Energy Phys. 08 (2012) 074.
[145] M. Badziak, M. Olechowski, and S. Pokorski, J. High Energy Phys. 06 (2013) 043.
[146] U. Ellwanger, J. F. Gunion, and C. Hugonie, J. High Energy Phys. 02 (2005) 066.
[147] R. Harnik, G. D. Kribs, D. T. Larson, and H. Murayama, Phys. Rev. D **70**, 015002 (2004).
[148] C. G. Lester and D. J. Summers, Phys. Lett. B **463**, 99 (1999); Y. Bai, H.-C. Cheng, J. Gallicchio, and J. Gu, J. High Energy Phys. 07 (2012) 110; A. J. Barr, B. Gripaios, and C. G. Lester, J. High Energy Phys. 11 (2009) 096; P. Konar, K. Kong, K. T. Matchev, and M. Park, J. High Energy Phys. 04 (2010) 086.
[149] D. R. Tovey, J. High Energy Phys. 04 (2008) 034.